Hydrogeochemical Analysis and Weathering of Monteagle Limestone: Tumbling Rock Cave, Northeast Alabama

by

Bailey Michael Martin

(Under the direction of Todd C Rasmussen)

Abstract

Karst landscapes have unique hydrological features and susceptibility to rapid dissolution, contamination and unpredictable groundwater flow, especially in carbonate rock. In these regions surface water availability is limited, causing groundwater to be the primary source for drinking water and irrigation. This study focuses on understanding the dissolution of carbonate rock, surface-groundwater interactions, and water quality within Tumbling Rock Cave, Alabama. This research utilizes a variety of analytical methods to characterize the carbonate rock and water quality within the cave, but also to understand the surface-groundwater interactions and make predictions about calcite dissolution. Results from this study aim to contribute to the elementary field of karst hydrology by predicting water availability and quality, and to provide broader implications for managing these vital resources.

Index words: Karst Hydrology; Monteagle Limestone; Tumbling Rock Cave; Southeastern Cave Conservatory, Inc.

Hydrogeochemical Analysis and Weathering of Monteagle Limestone: Tumbling Rock Cave, Northeast Alabama

by

Bailey Michael Martin

B.S. Environmental Resource Science, University of Georgia, 2020

A Thesis Submitted to the Graduate Faculty

of The University of Georgia in Partial Fulfillment

of the

Requirements for the Degree

Master of Science

Athens, Georgia

2023

Hydrogeochemical Analysis and Weathering of Monteagle Limestone: Tumbling Rock Cave, Northeast Alabama

by

Bailey Michael Martin

Approved:

Major Professor: Todd C Rasmussen

Committee: Charlotte Garing
Nandita Gaur

Electronic Version Approved:

Ron Walcott
Interim Dean of the Graduate School
The University of Georgia
December 2023

Acknowledgments

I would like to acknowledge and express my gratitude to a few individuals who helped make this research possible. I would like to first thank my parents, Troy and Leslie Martin, my sister Caroline Martin, and all of my family for the unwavering support throughout graduate school. I would like to thank my girlfriend, Carleigh Ellison, for pushing me to be my best and helping me manage the stress of graduate school. I would like to thank all of my friends, old and new, who have encouraged and motivated me throughout this journey. I would specifically like to thank two friends, Tommy Bilkey and Carly Daniel, who made the journey to my field site and assisted in field sampling and sample preparation. A profound thank you to my advisor, Todd Rasmussen, for all of the help, kindness and support throughout my journey in graduate school. I would also like to thank my committee members, Dr. Garing and Dr. Gaur, as well as my colleagues and friends in this program for supporting me and helping me throughout graduate school and allowing me to be standing here in front of you today. This program and research would not have been possible without all of my support. I am so thankful for the last five years I have spent at the University of Georgia and all that this institution has given me.

Table of Contents

List of Tables

List of Figures

Chapter 1

Introduction

1.1 Motivation

Karst landscapes are known for their abundance of carbonate rocks that support active subsurface groundwater movement, thus limiting surface-water availability. Karstic regions of the globe are typically rich in bedrock outcrops, sinkholes, caves, sinking streams, and rocky terrain. Carbonates are prone to rapid dissolution through chemical and physical interactions with water. Groundwater in karst landscapes is notably susceptible to unpredictable flow and contamination. Water resources in these regions can be difficult to characterize and interpret due to the complexity of dual-porosity subsurface infiltration. Management of these resources is vital because it serves as the main source of drinking water and irrigation for much of the global population.

1.2 Karst Formations

Karst landscapes are formed by the dissolution of soluble bedrock. Chemical weathering of carbonate rocks (e.g,, limestone, dolomite, marble) creates underground conduits that promote subsurface drainage, sinkholes, and vast caverns (Groves and Meiman 2005). Over geologic time, these areas become layered with differing rock and mineral types creating extensive hydrologic connectivity between the surface and subsurface.

Karst landscapes typically lack surface water because of the large fractures and caverns below. Because of this, quantifying and extracting water can be difficult to accomplish

without adequate technologies. Karst landscapes are also highly susceptible to groundwater contamination because of the rapid flow and permeability of the rock.

Karst landscapes are typically characterized by analyses of parent rock, water quality, groundwater recharge, and transport and modeling.

1.3 Problem Statement

Karst landscapes are formed from the dissolution of permeable bedrock, where surface water is substantially devoid, leading to the formation of vast conduits, caverns, and caves. The hydro-connectivity of these regions permits the resources to be vulnerable to water quality problems from runoff such as oil spills, high pesticide and fertilizer concentrations, and bacteria (Currens 1999). Currently, the management of karst landscapes is minimal and lacks sufficient resources to characterize surface-groundwater interactions.

The Southeastern Cave Conservancy (SCCi) is a non-profit organization that currently manages over 170 caves and serves as the largest land conservation exclusively focused on cave protection. SCCi seeks to preserve and identify the best management strategies for these natural wonders. Tumbling Rock Cave, in Jackson County, Alabama, is owned and managed by SCCi. Figure 1.1 illustrates a cave density map of the southeastern United States, demonstrating Jackson County, Alabama having the greatest cave density in the Kentucky, Tennessee, Alabama, and Georgia (KTAG) region. Tumbling Rock Cave (TRC) serves as the ideal field site, not only because of the resources the SCCi provides but also their dedication to educating and informing the public. TRC had over 3500 visitors in the 2023 Water Year (Oct 2022 through Sept 2023).

The goal of this study is to characterize limestone dissolution, surface water-groundwater interactions and water quality issues in Tumbling Rock Cave. With this information, we can better understand interactions between the surface and subsurface and make predictions on water availability and quality.

1.4 Research Hypotheses and Objectives

This research focuses on developing and evaluating procedures for karst groundwater characterization by examining rock-water interactions. We hypothesize that:

1. The vulnerability to contamination in karst landscapes is a function of travel (or residence) times in the subsurface, with shorter residence times being more susceptible to contamination than longer pathways with greater residence times.
2. Rock elemental composition affects weathering rates through calcium dissolution so that water with longer subsurface travel times have greater calcium content than faster pathways.
3. Other water quality parameters (e.g., pathogens) are also affected by travel times, so that measuring carbonate concentrations provides information about the vulnerability to groundwater contamination.
4. Types of subsurface flows (rapid flow through streams in conduits, fracture, and drip flow) are related to travel times, so that knowledge of calcium concentrations from each provides information on their respective travel times.

Specific research objectives include:

1. Characterize parent rock material using X-ray diffraction (XRD), acid digestion, and laboratory mineral weathering procedures.
2. Characterize groundwater quality from precipitation, drips, subsurface streams, and spring discharge using Atomic Absorption Spectroscopy (AAS), Inductively Coupled Plasma - Mass Spectrometry (ICP-MS) (i.e., Al, Ca, Fe, K, Mg, S), and chemical water quality parameters.
3. Use dissolved calcium concentrations to indicate calcite dissolution.

4. Estimate how temperature affects calcite dissolution rates from limestone samples using laboratory mineral weathering procedures and geochemical modeling.

1.5 Organization

Following this introduction, Chapter 2 summarizes the literature and provides a detailed overview of the Tumbling Rock Cave, its geological features, hydrology, topography, soils, land cover, and the analytic methods used for studying it. This chapter provides a comprehensive introduction to the field site and introduces the research and types of analyses in subsequent sections. Chapter 3 presents the methodology and analyses used in this study. This chapter provides an overview of the field, laboratory, and modeling procedures utilized in this research. The field research introduces insight into the stream flow, water quality, and meteorologic data.

Laboratory data focuses on the simulated mineral weathering procedure and the types of analyses performed using field samples. The modeling section introduces batch reaction equations used for geochemical modeling, involving rates of reactants changing in concentration over time. Chapter 4 describes the results and implications of the data collected, while Chapter 5 concludes this thesis with a discussion of management and future research needs.

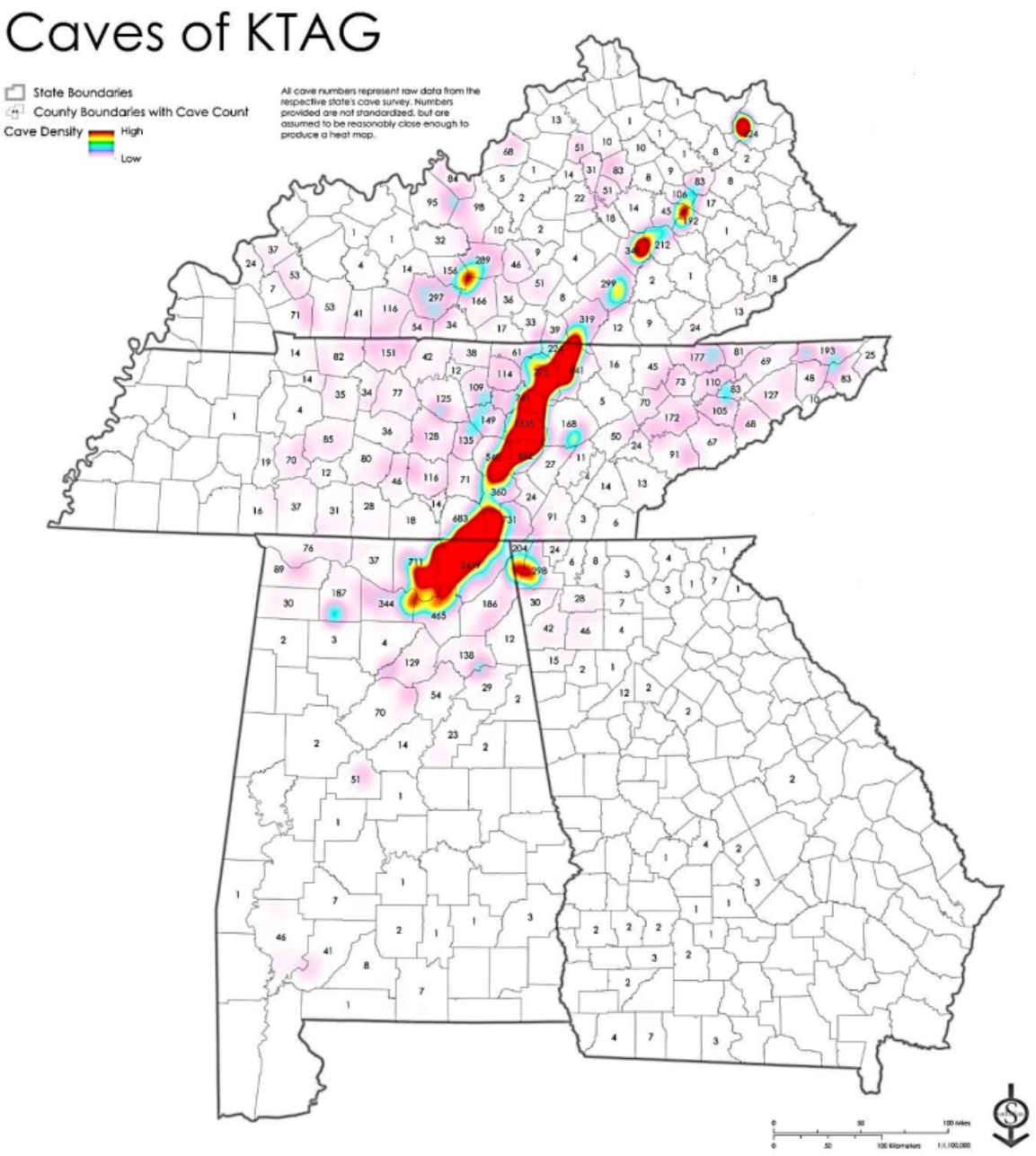

Figure 1.1: Cave density map of the Kentucky, Tennessee, Alabama, Georgia (KTAG) region of the Southeast United States modified from (Sutherland, 2021)

Chapter 2

Literature Review

2.1 Previous Studies

Previous work on Tumbling Rock Cave by Zachary Normile and Dr. Rasmussen have identified a number of water quality and flow parameters within the cave. Their studies focused on investigating the presence of coliform and E. Coli within drips and streams, which would indicate surface water recharge. Normile's research identified greater contamination in the conduits and longer residence times in the drips. Normile measured concentrations of E. Coli and specific conductance between the conduits (rapid flow) and drips (slow flow). This research identified greater contamination (E. Coli) in the conduits and greater specific conductance in the drip samples (Normile 2022). This work leads us to believe, that drips (slow flow) have longer residence time and greater rock-water interactions. Normile also mapped much of the cave using a light detection and ranging (LiDAR) backpack that was able to precisely image the main passageway and channels throughout the cave. Dr. Rasmussen's research looked at response times between precipitation and flow within the cave. Various other studies at the University of Georgia (UGA) looked at air quality and airflow within the cave.

2.1.1 Surface-Groundwater Interactions

Surface water-groundwater interactions dictate the formation of fractures, conduits, and ultimately cave systems. Surface water can infiltrate the subsurface in a number of ways, e.g., soil percolation, sinkholes, and sinking streams. Surface water can transport ions and

contamination during recharge periods. This changes the water quality of the groundwater and can lead to dissolution.

2.1.2 Cave Drips

In cave systems, ceiling drips are often responsible for the formation of speleothems because of their high calcium concentrations. As dissolution occurs in the rock above, calcium concentrations accumulate before exiting the host rock as ceiling drips. Speleothems are the classification for cave decorations, such as stalagmites, stalactites, soda straws, curtains, etc., formed from the precipitation of calcium ions. Studies have shown how the flow and water quality of ceiling drips can differ based on seasonal variability. A study on carbonate rock in Ireland shows that calcium concentrations in drips increased during low flow and decreased during high flow (Tooth and Fairchild 2003) The increased flow is believed to occur shortly after precipitation events, when recharge is at its peak. The decreased concentrations of calcium are likely to be from dilution during these events.

Other studies have looked into how drips change over time. A study on cave drips in the Mediterranean Sea found that water quality within drips can change due to the type of cave drips, perennial, seasonal, post-storm, and overflow (Arbel et al., 2010). This study used dye tracers to understand the flow velocities during different drip events. This study also looked at the chloride concentrations in the water to determine flow type and differentiate old and matrix water. This study found that almost 25% of flow was preferential flow.

2.1.3 Leachate Transport

Column studies coupled with modeling can be utilized to characterize and predict leachate transport in a number of environmental systems. This is typically done in order to understand water quality discharge at a mine site or landfill. These column experiments are performed by controlling a number of variables such as, flow, humidity, temperature, etc... These experiments are done by filling columns with soil or rock material and (continuously or cyclically)

leaching in order to characterize the water quality of the leachate. These studies are able to show how physical, geochemical, and biological interactions can affect leachate transport (Islam and Naresh 2004).

2.2 Field Site Description

Tumbling Rock Cave, owned and managed by the Southeastern Cave Conservancy (SCCi), is dedicated to promoting education on caves while protecting and conserving these natural wonders. Tumbling Rock Cave is located in Jackson County, Alabama about 20 km south of Tennessee and 45 km west of Georgia. The cave entrance sits at the base of a mountain known as Buzzards Roost Peak (Crow Mountain), Alabama. This SCCi site has power and internet connectivity which makes it an ideal location for this study. This cave has one known entrance and approximately 10 km of mapped passageways, names listed in Table 2.1. This site offers guided trips as well as training opportunities for cave search and rescue. Tumbling Rock Cave was also utilized for mining in the late 1800s. During the Civil War, saltpeter, a mineral containing potassium nitrate, was mined for the manufacturing of gunpowder.

2.2.1 Geology

The geology of Alabama is comprised of four major geologic eras. The eras consist of the Cenozoic in the south coastal plain, the Mesozoic in the middle of the state, the Precambrian in the Piedmont, and the Paleozoic in the north (Adams et al., 1926). The geologic types and formations are shown in Figures 2.1, 2.2, and 2.3.

Globally, karst terrain is dominated by carbonate rock, primarily composed of limestone or dolomite (White 1988). The karst geology of the Southeastern United States was predominantly influenced by the Mississippian and Pennsylvanian periods. These formations vary in composition, containing sandstones, mudstones and limestones shown in Table 2.2. The most prominent formation in Northeast Alabama, and Tumbling Rock Cave, is Monteagle Limestone. “The Monteagle Limestone (Genevievian and Gasperian Stages) consists

of shallow-water carbonate deposits organized into shoaling upward parasequences" (Thomas and Mack 1982).

Figure 2.1 depicts the geologic quadrangle adjacent to the field site. The Geological Survey of Alabama, Scottsboro Quadrangle Q63 identifies the geologic types and provides a cross-section with consistent lithology to that of Tumbling Rock Cave. Although there is no geologic quadrangle for the field site, the geologic formation layers and depths in Q63 are consistent with the field site and literature on the Cumberland Plateau Geology.

Similar geology stretches in the northeast direction from North Alabama into most of Kentucky. This area is known as the Cumberland Plateau, one of five geographic regions of Alabama. The carbonate rock in this region is susceptible to chemical weathering. Desiccation of partly consolidated sediments and dissolution of evaporites in the Cumberland Plateau results in sediment collapse, ultimately leading to voids and cracks filled by calcite (Hanford 1978).

Many rock formations within the cave are shaped by water and/or subsurface airflow. The cave is diverse in stalagmite, stalactite, and column formations that range from a few centimeters to several meters tall. The cave also features a 121 m (396 ft) waterfall known as "Topless Dome". The extent of the cave passageway runs almost excessively through the Monteagle limestone. Limestone is a type of soft carbonate rock that is easily weathered given the appropriate water quality and flow conditions. The abundance of rock formations, conduits, and an active underground stream leads us to believe the rock material within the cave is susceptible to dissolution. Another prominent feature is active petroleum seepage in the "back" of the cave.

2.2.2 Hydrology

Karst landscapes are influenced by quick responses to surface precipitation followed by short residence times. Over thousands (often millions) of years, mechanical and chemical weath-

ering from hydrologic events are responsible for the formations present in karst. Groundwater recharge and discharge are the main components of water movement in karst. Cave discharge can easily be quantified at the resurgence (spring head), however, cave inputs can be more difficult to characterize. Generally, rainfall is the greatest source of groundwater recharge, with little movement from surface streams (Chu et al., 2017).

Recharge can occur from four different mechanisms, allogenic recharge, diffuse infiltration, internal runoff, and overflow from perched aquifers (White 2002). Allogenic recharge occurs when surface water runs off non-karst landscapes onto karst landscapes where it enters the subsurface through depressions, sinkholes and fractures. Diffuse infiltration occurs when precipitation directly falls on carbonate rock and recharges the aquifer through soils, fractures or matrix bedrock. Internal runoff is similar to overland flow, in the sense that rainfall accumulated on the karst landscape infiltrates quickly through depressions and sinkholes. The final recharge mechanism occurs when water bodies accumulate in the vadose zone due to low permeability layers. The perched aquifer eventually reaches a capacity where it drains into the karst subsurface.

Groundwater movement through karst subsurfaces can occur in several manners, through the rock matrix, rock fractures, and conduits. Darcy's Law describes groundwater flow through an aquifer by defining the flux (the flow rate per unit area) as the product of the hydraulic conductivity (or permeability, which is the ability of water to pass through media) and the hydraulic gradient (the change in total head with distance). Groundwater flow behavior in karst aquifers differs from Darcy's law due to the large number of preferential flow through the karst network that precludes traditional porous media flow (Panagopoulos and Lambrakis, 2006).

Water movement tends to follow the easiest flow paths. Over time, these flow paths become preferential flow networks, increasing in volume as dissolution occurs. In karst, these networks create drips, fractures, or even large conduits that can transport large volumes of water. This

is where most of the recharge, dissolution, and flow ultimately converge. Movement through the rock matrix is generally slow but dependent on the rock's porosity and permeability.

Fracture flow typically exhibits a faster response to precipitation events than other groundwater sources. This type of flow typically identifies areas where there is a significant hydrologic connection with the surface. Because of these mechanisms, the rock matrix is responsible for storage and water-rock interactions, while the fracture flow facilitates the transport of solutes. (Neven and Sorab 2021).

Fracture flow increases after substantial precipitation, while water typically recharges laterally through the soil and rock matrix after lesser precipitation events. Flow and hydrologic connectivity varies seasonally due to differing rates of evapotranspiration and soil moisture (Baker et al., 1997). Fracture flow is dominant during the wetter months with lesser recharge during drier months.

Although surface water is minimal in karst landscapes, it is responsible for most of the recharge, organic inputs, and contamination. Because of the rapid connection of streams through sinkholes, most ion concentrations see an increase from upstream to downstream and a further increase into groundwater (Wu et al., 2007). The introduction of these ions can provide nutrients for organisms within the cave, but also create acidic conditions, furthering dissolution.

Figure 2.4 shows a conceptualized cave system where slow-moving transport is indicated in blue and fast-moving conduits and underground streams are indicated in red.

Tumbling Rock Cave sits in a valley that is fed by a variety of water sources. Mud Creek is the most predominant surface water stream in this watershed. Mud Creek is formed in the foothills of the valley where it continues to accumulate flow in the southeast direction The entrance to the cave, or spring head is the next largest contributor to surface water. The spring head emerges at about 200 m above mean sea level (AMSL) where it joins Mud Creek. Mud Creek continues to flow in the southeast direction, where it converges with other streams

to become Tennessee River and eventually Guntersville Lake. Because Tumbling Rock Cave sits in a steep valley, most of the precipitation in the valley contributes to Mud Creek as runoff, where some will seep into the subsurface and become groundwater.

A stream follows the main passageway. A variety of ceiling drips feeds this stream, and inflows from fractures and tributary conduits. Previous studies at this site have identified water quality issues, such as fecal contamination, which lead us to believe there are numerous interactions with surface water, as there is minimal animal activity within the cave. The large waterfall within Topless Dome has also seen rapid responses in flow due to localized precipitation events. Previous studies by Dr. Rasmussen at UGA have shown a significant response in Topless Dome following large precipitation events.

The contributing watershed for Tumbling Rock Cave was delineated using USGS StreamStats, accounting for 12.84 km^2, shown in Figure 2.5. The USGS StreamStats tool delineates a watershed based on a single geographic point. The software is intended to utilize the surrounding topography to determine the drainage area. This software struggles to account for karst landscapes, especially sinkholes and depressions. The result can incorporate unconnected streams, invalid recharge areas, and create flow paths up gradient, inconsistent with the landscapes' hydrologic characteristics. This is one of many indications that this landscape is in karst, emphasizing the fact that these regions remain under-researched.

2.2.3 Soils

Soil data was accumulated utilizing Web Soil Survey for the delineated watershed generated from USGS Streamstats. The total area of interest accounted for 20.67 km^2 (2,067.34 ha). The program identified thirteen different types of soil cover within the watershed, the most notable including Nauvoo fine sandy loam (34.1%), Rocky Stony Land, Muskingum (18.9%), Muskingum fine sandy loam at (15.7%) and Limestone rock land (11.3%), described in Table 2.3.

The abundance of exposed limestone and "rock" on the surface is another indication of a karst landscape. While karst landscapes are predominantly known for generating clay-rich soils, the overlying soil of this region is primarily sandy loam. Sandy loam soils are distinguishable from clays and silts because of their permeability. Sandy loam soils facilitate rapid recharge compared to other soil types. Soil quality is largely responsible for driving groundwater recharge and water quality in karst landscapes. This area and the surrounding valleys are more suitable for harvesting compared to the rolling hills and slopes of surrounding regions (Schweitzer 2013). Sandy soil in the Cumberland Plateau serves as ideal farmland during wetter months of the year due to infiltration rates of sand and the flat surface of the region.

2.2.4 Topography

The entrance to Tumbling Rock Cave is located 200 m asl. It sits at the base Buzzard Roost Peak, Alabama which is about 500 m amsl. The cave fluctuates vertically in elevation throughout the breadth of the main channel but overall rises from the entrance towards the back of the cave. The cave sits in the southern region of the Cumberland Plateau, which extends northeast into much of Tennessee, Georgia, and Kentucky. This region is known for being largely flat and elevated above the surrounding regions. The Cumberland Plateau is comprised of Pennsylvanian age sediment nearly 2 km thick. (Swingle 1965). The Cumberland Plateau and topography of the field site are illustrated in Figure 2.6.

2.2.5 Land Cover and Use

Land use for the Tumbling Rock Watershed is dominated by deciduous forest, followed by areas of pasture, shrub, barren land (rock/sand/clay), evergreen forest with limited amount of surface water, and urban development. The majority of the land surrounding the cave is dedicated to agriculture and hunting lands.

2.3 Geochemical Modeling

Simulation of geochemical interactions between water and rock over space and time can also be performed using a variety of numerical tools. This section describes the methods used in this study.

2.3.1 PHREEQC

PHREEQC is a free geochemical modeling software available from the USGS, PHREEQC Version 3 (USGS 2021). This program allows you to perform a number of geochemistry calculations including, but not limited to ion dissociation, mineral precipitation, and ion transport. In this study, PHREEQC is utilized to determine the kinetics for dissolution, and the equilibrium kinetics and predict concentrations of dissolved calcium in a batch reaction at various temperatures.

2.3.2 Mineral Weathering

Carbonate minerals, especially calcite, have higher dissolution rates than other minerals. The reaction occurs by the consumption of a free hydrogen ion, releasing a carbon ion and a carbonate. (Li et al., 2007). The rate of dissolution is directly proportional to the activity of the hydrogen ion at low pH, while at higher pH the rate decreases due to the backward precipitation reaction (Chou et al., 1989). A number of calcite dissolution reactions can occur, based on the concentration of calcium ions, temperature, pH, and conditions of the water. Dissolution of calcite happens simultaneously in three different reactions based on these conditions. (Chou et al., 1989; Plummer et al., 1978)

$$CaCO_3(s) + 2H^+ \Longleftrightarrow Ca^{2+} + H_2CO_3 \tag{2.1}$$

$$H_2CO_3 \Longleftrightarrow H^+ + HCO_3^- \Longleftrightarrow 2H^+ + CO_3^{2-} \tag{2.2}$$

$$CaCO_3(s) \Longleftrightarrow Ca^{2+} + CO_3^{2-} \tag{2.3}$$

The chemical reactions above describe different outcomes for carbonate dissolution and precipitation. Equation 2.1 describes calcium carbonate dissociating into free calcium ions and carbonic acid. In this reaction, solid calcium carbonate dissociates into a carbonic acid due to acidic conditions because of the excess H^+ ions.

Equation 2.2 describes the carbonic dissociating into free H^+ ions and a bicarbonate. Equation 2.3 describes the dissolution of calcium carbonate into free Ca^{2+} ions and carbonate ions in the water. Equation 2.3 is likely what we will see occurring within the cave, and directly be able to measure the abundance of free Ca^{2+} ions.

The transport rate and kinetic rate of dissolution can be determined by understanding the solubility and the equilibrium constants. It is important that when we consider these equations there are a number of factors that dictate this reaction such as pressure, temperature, pH, initial calcium concentration, and the presence of other minerals. Throughout this study, we will investigate how some of these parameters affect the rates of dissolution.

2.4 Experimental and Analytic Methods

There are a wide variety of methods for characterizing rock elements and minerals. This section describes the methods used in this study.

2.4.1 Mineral Forms (XRD)

X-ray diffraction (XRD) is an analytical method used to determine the mineralogical composition and structure of solid materials. This instrument is able to measure the solid structure by sending X-rays through the sample into an X-ray detector. As each of the rays is sent through the sample, light is refracted or bent due to collision with solid material. The X-ray detector is able to detect the magnitude of diffraction to map an image of the sample. XRD is able to identify crystalline structures by measuring the shape, size, and orientation of the

crystals. Computer software is able to refer to known mineralogical structures to determine the minerals present in each sample.

2.4.2 Acid Digestion

Acid digestion is utilized on soils, rocks, and metals depending on the goal of the analysis. This method is often employed for analytical and characterization purposes. In this study, rock samples are analyzed for elemental concentrations through an acid digestion procedure. This technique uses a strong acid to dissolve the solid material leaving behind the elements of interest. The reaction is performed by placing samples into microwave vessels containing Nitric acid. The vessels are then inserted into a digester at 200°C for 30 minutes. The digested samples are then ready to be tested for elemental composition following a dilution with 100 mL of DI water.

2.4.3 Elemental Analysis (ICP-MS and ICP-OES)

Inductively Coupled Plasma–Mass Spectrometry (ICP-MS) is a technique used to measure trace amounts of elements in liquid, solid, or gas samples. This instrument is utilized in a variety of different studies ranging from water quality to radiocarbon dating. The instrument is able to measure specific isotopes at low detection limits by a mass-charge ratio. The dissociated instrument is first calibrated by known amounts of an element to determine calibration curves. The instrument can then determine the concentration of an element by correlating counts of an isotope to the calibration curve. Most samples must be diluted to accurately quantify the concentrations because of the instrument's ability to detect at low detection limits (Lin et al., 2016).

Inductively Coupled Plasma - Optical Emission Spectroscopy (ICP-OES) is an analytical technique similar to ICP-MS. ICP-OES is performed to determine elemental concentrations of solutions. ICP-OES is different from ICP-MS in the way concentrations are determined. ICP-OES excites ions and measures their wavelength. This is done by heating liquid samples

with a plasma, releasing electrons as photons that give off a unique wavelength for a given element (Olesik 1991).

2.4.4 Atomic Absorption Spectroscopy (AAS)

Atomic Absorption Spectroscopy is an instrument that detects concentrations of elements based on the wavelengths they emit. The solid or liquid of interest is rapidly heated to 2000-3000°C. At this temperature, elements absorb a concentration of the wavelength given off by the flame. A cathode lamp produces a laser that is able to identify the absorption wavelength and intensity to determine the concentration of an ion.

Table 2.1: Glossary of Tumbling Rock Cave place names

Allens Alley. Large passage beyond the Blue Crawl that was first explored by Jack Allen in 1960

Asphalt Pool. A patch of oil in the upper level that parallels the Kings Shower

Asphalt Ooze. Patches of substance that is probably asphalt that has dripped from the ceiling. The phenomenon is located on breakdown blocks located at the uppermost slope in the Hall of the Gods

Blue Crawl. Nittany Grotto cavers noticed that the air turned blue from invectives emitted by cavers as they squeezed through the tight crawl connecting the Emperor's Room with the Inner Sanctum during a trip in the 1960s.

Christmas Tree. A distinctive flowstone stalagmite located in the Great Hall of Mysteries

DT Passage. The breakdown between Mt-Olympus and Grant's Torch named after Peter Dowell and Terry Tarkington, the cavers who originally pushed through the crawL

Elephants Feet. Large circular formations located beyond the Saltpeter Works named by Stevenson in 1957

Fishreel Canyon. During the Huntsville Grotto's first trip in 1953 they lost a fish reel with the survey tape on it in this canyon (recovered since).

Ghost Crawl. A group of Huntsville Cavers with a dog were mapping the cave in 1956. On the way out, Bill Varnedoe swears that the dog kept behind him and kept touching his back while he was in a crawlway. Once out of the crawl, however, Bill saw that the dog was not behind him in but front of him, The caver behind Bill reports that the dog was never behind him in the crawl nor was there anything touching Bill. Rather than accept this account, Bill named the passage Ghost Crawl.

Great Hall of Mysteries. A large chamber beyond the King's Shower named because of mysterious holes in the ceiling.

Hall of the Gods. Several hundred feet of borehole that leads to Mount Olympus and the Pillar of Fire

Hidden Door. Located just beyond the Totem Gallery, the unobvious but nevertheless main route "Door" is remarkable. It can be difficult to find in the breakdown when exiting the cave.

King's Shower : The original access to Topless Dome was through a waterfall located in the side passage across from the Topless Dome. The new access route to Topless Dome was created by knocking a hole in the ceiling of the main passage, which diverted the waterfall through the new opening

Pillar of Fire, Flamingoes. A large, bright red and orange stalagmite located at the top of Mount Olympus. The Flamingoes are two red stalagmites at its base.

Table 2.1 (continued).

The Sewers. A series of breakdown and wet crawls located on the west side of the mainstream before the Wildcat Rockpile
Terrys Terrible Tiger Teeth. A distinctive set of Ioose looking rocks that hang from the ceiling in a breakdown passage near the end of the cave.
Topless Dome. A 129-m (396-ft) high gun-barrel shaped dome accessed through King's Shower.
Suicide Passage. An unstable breakdown pile that used to be the terminus of cave. It has since been excavated and stabilized to bypass the Blue Crawl.
Vujade Extension : An upper-level passage located above the Elephants Feet named because footprints indicated that "everyone else" had been there before the team who mapped it.

Table 2.2: Age and thicknesses of geologic formations within the Cumberland Plateau, NE Alabama (Thomas, 1972).

Geologic Period	Formation	Thickness (m)	Geologic Age (yrs before present, millions)
Pennsylvanian	Pottsville	15 - 24	<318
Mississippian	Pennington	30 - 45	318 - 320
	Bangor Limestone	60 - 75	320 - 328
	Hartselle Sandstone	12 - 18	328 - 330
	Monteagle Limestone	45 - 60	330 - 340
	Tuscumbia - St. Louis Limestone	>45	>340

Table 2.3: Major soil groups and their area within the Tumbling Rock Cave watershed (Web Soil Survey).

Symbol	Map Unit Name	Area (ha)	Area (%)
Ald	Allen loam, severely eroded, rolling phase	1.61	0.1%
BC	Barbourville-Cotaco fine sandy loams	1.54	0.1%
Bf	Bruno fine sandy loam	15.34	0.7%
Hfg	Hartsells fine sandy loam, 6 to 10% slopes, shallow	80.00	3.9%
Hfo	Nauvoo fine sandy loam, 6 to 10% slopes, shallow	704.80	34.1%
HnB2	Hartsells-Nauvoo complex, 2 to 6% slopes, eroded	42.73	2.1%
Jfn	Jefferson fine sandy loam, eroded, rolling phase	1.21	0.1%
Lr	Limestone rockland rough	234.07	11.3%
Mfl	Muskingum (Gorgas) fine sandy loam, 10 to 20% slopes, v stony	165.11	8.0%
Msl	Muskingum (Gorgas) stony fine sandy loam, 20 to 45% slopes, v stony	325.21	15.7%
Msz	Muskingum (Gorgas) stony fine sandy loam, 20 to 45% slopes, v stony	98.17	4.7%
RsM	Rough stony land, Muskingum soil material	390.24	18.9%
St	Sturkie fine sandy loam	2.95	0.1%
W	Water	4.33	0.2%
Total		2,067.34	100%

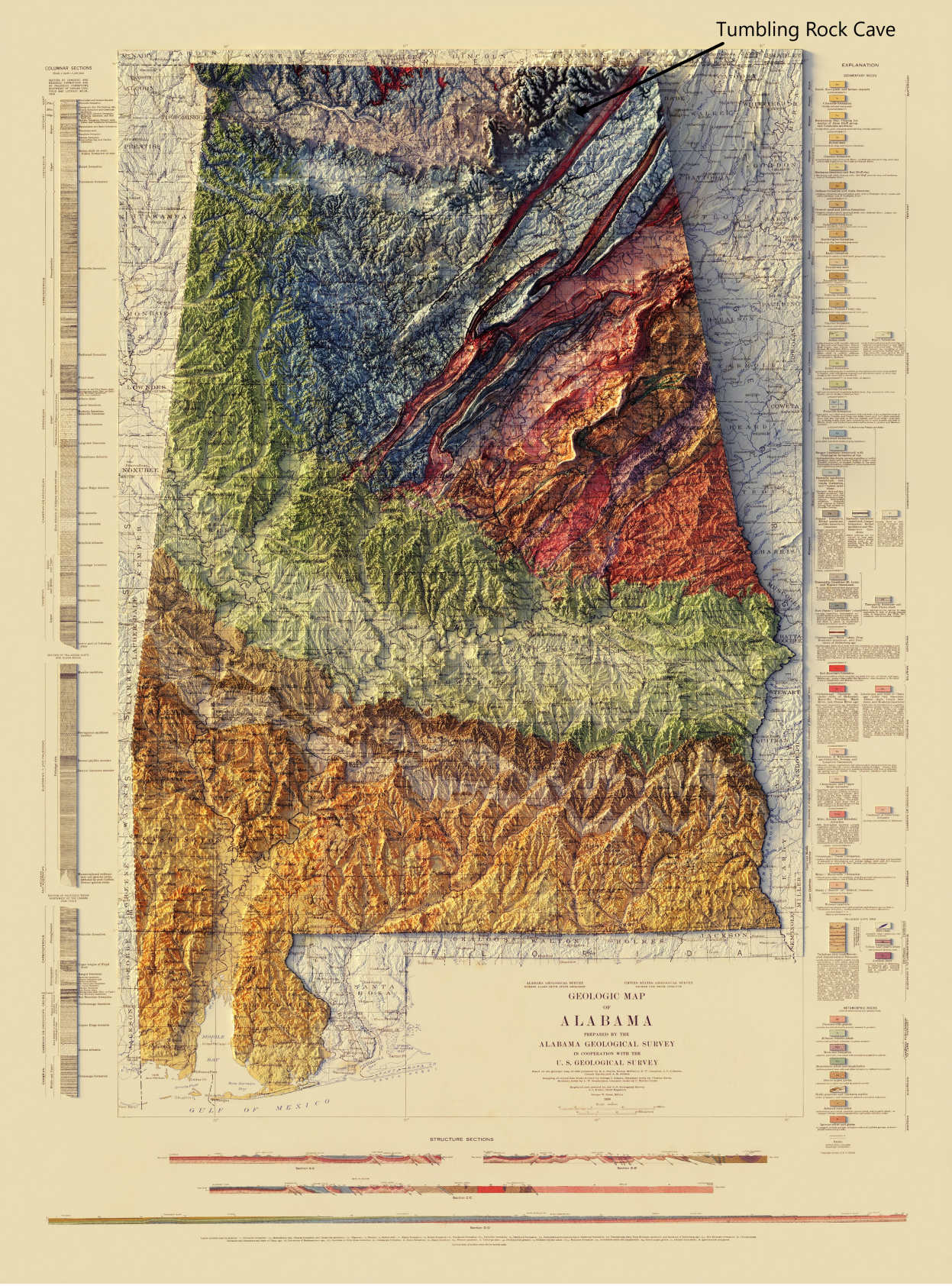

Figure 2.1: Geologic map of Alabama (modified from Sean Conway, USGS).

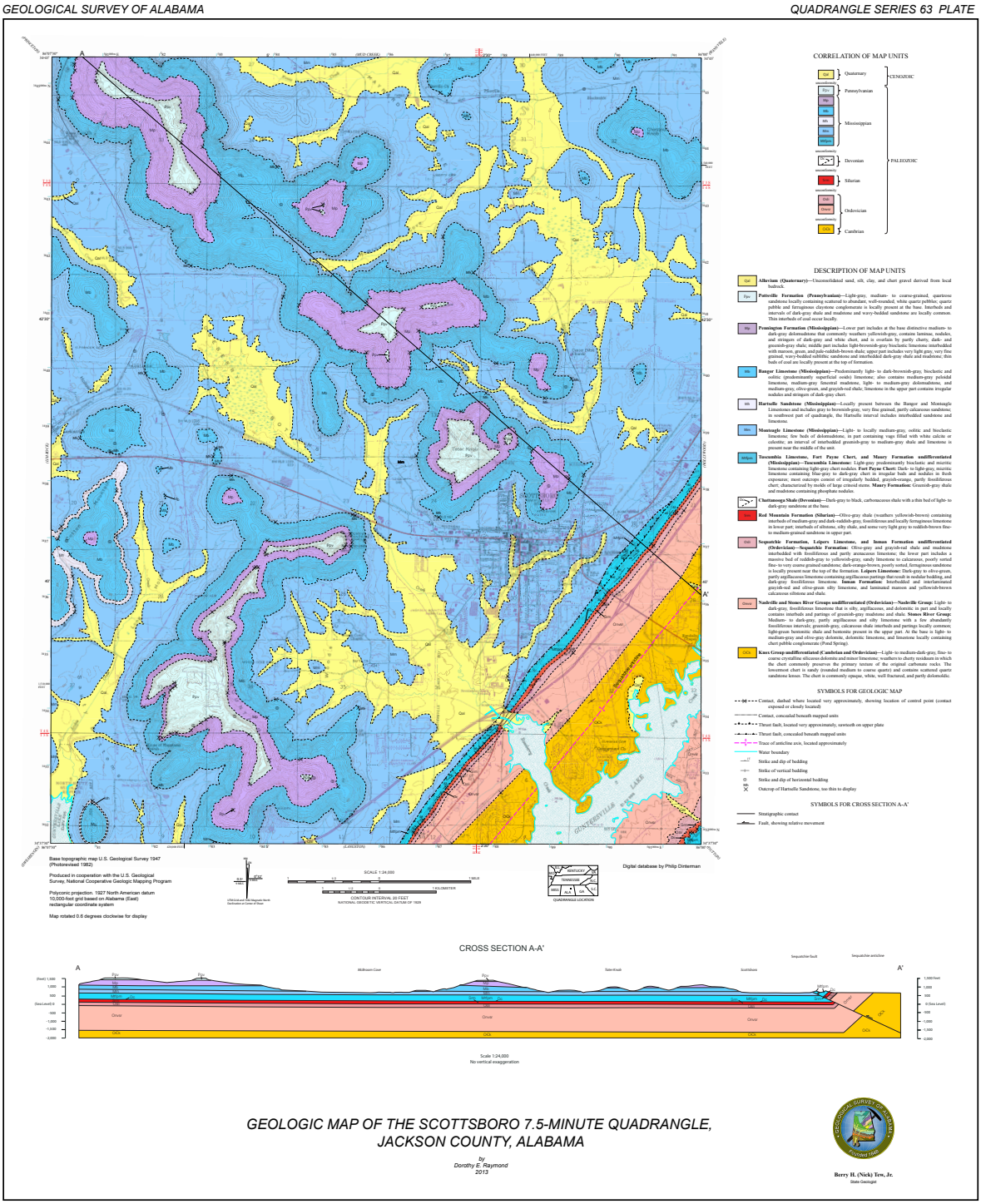

Figure 2.2: Geologic map and cross section, Scottsboro, Alabama, Quadrangle Series 63 (GSA, 2013)

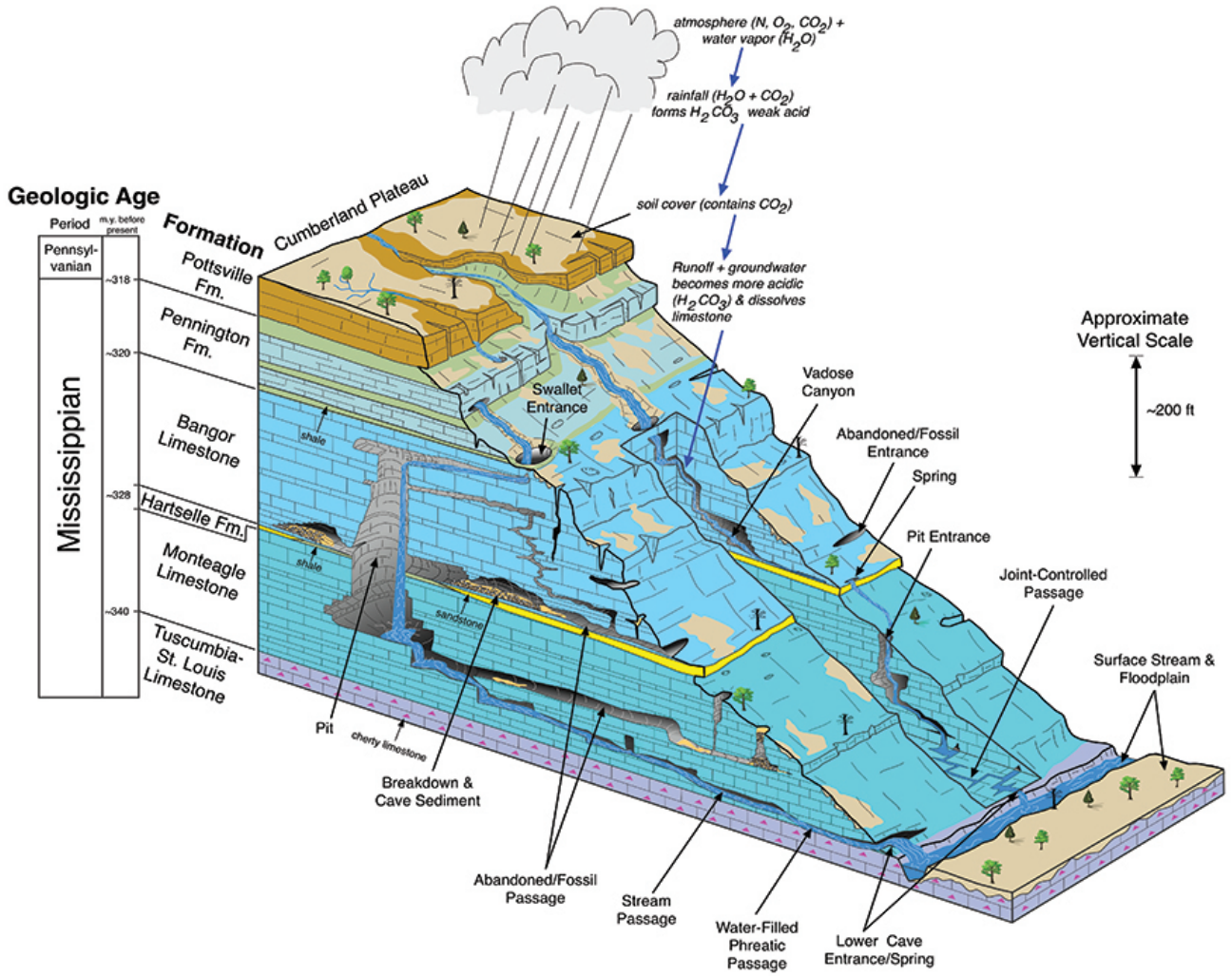

Figure 2.3: Geologic cross section of karst systems on the Cumberland Plateau, Southeast United States (SCCi, 2023).

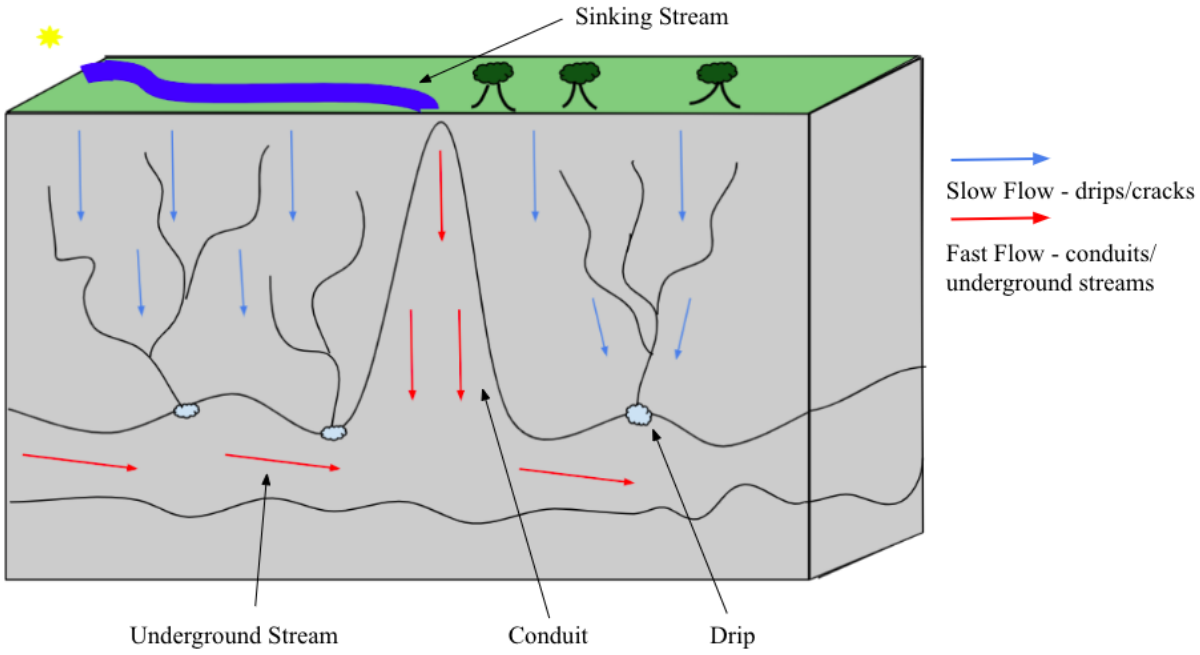

Figure 2.4: Conceptualized karst diagram indicating slow (fracture-drip) and rapid (channel-conduit) subsurface transport.

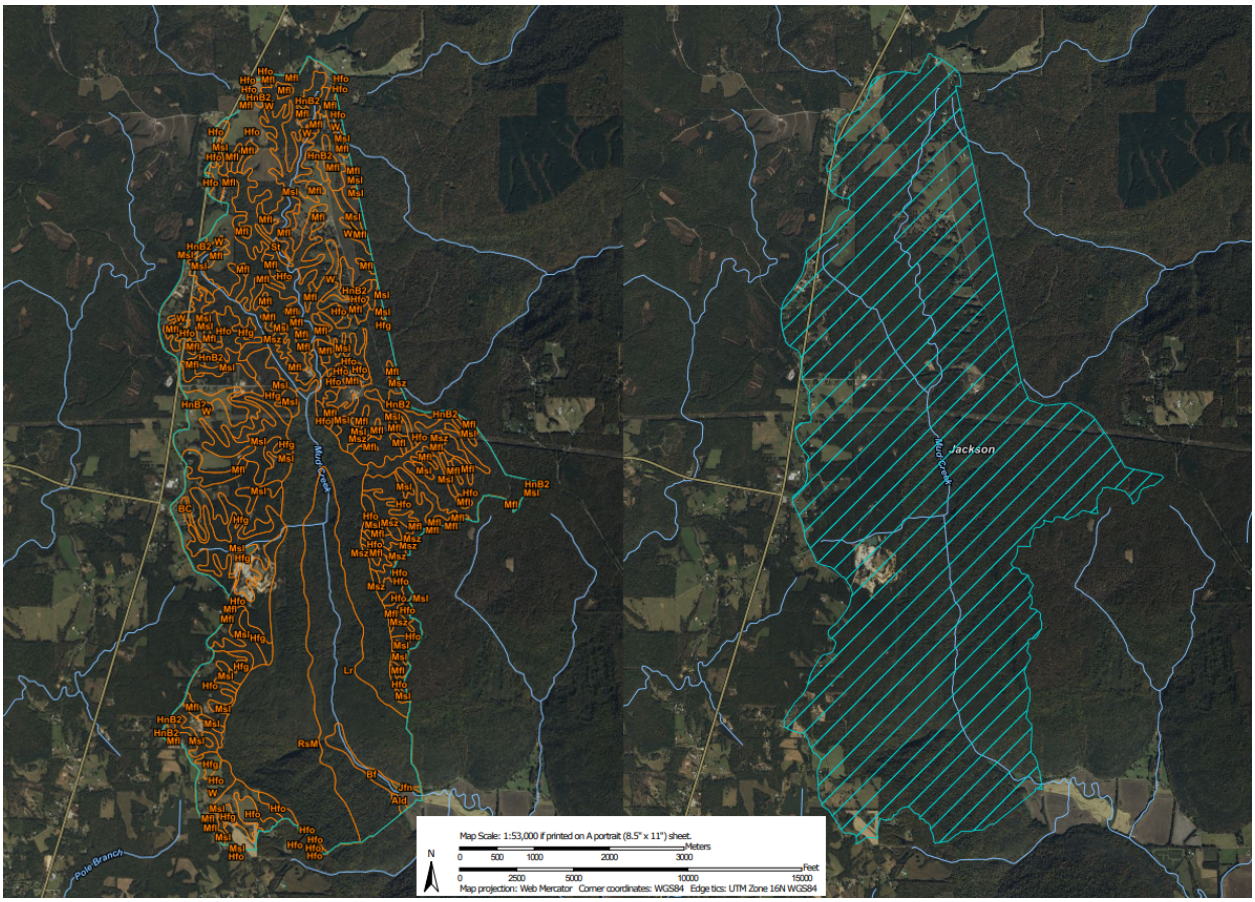

Figure 2.5: Soil map from Web Soil Survey (USDA-NRCS 2019) (left); Watershed map from USGS StreamStats (USGS 2023) (right).

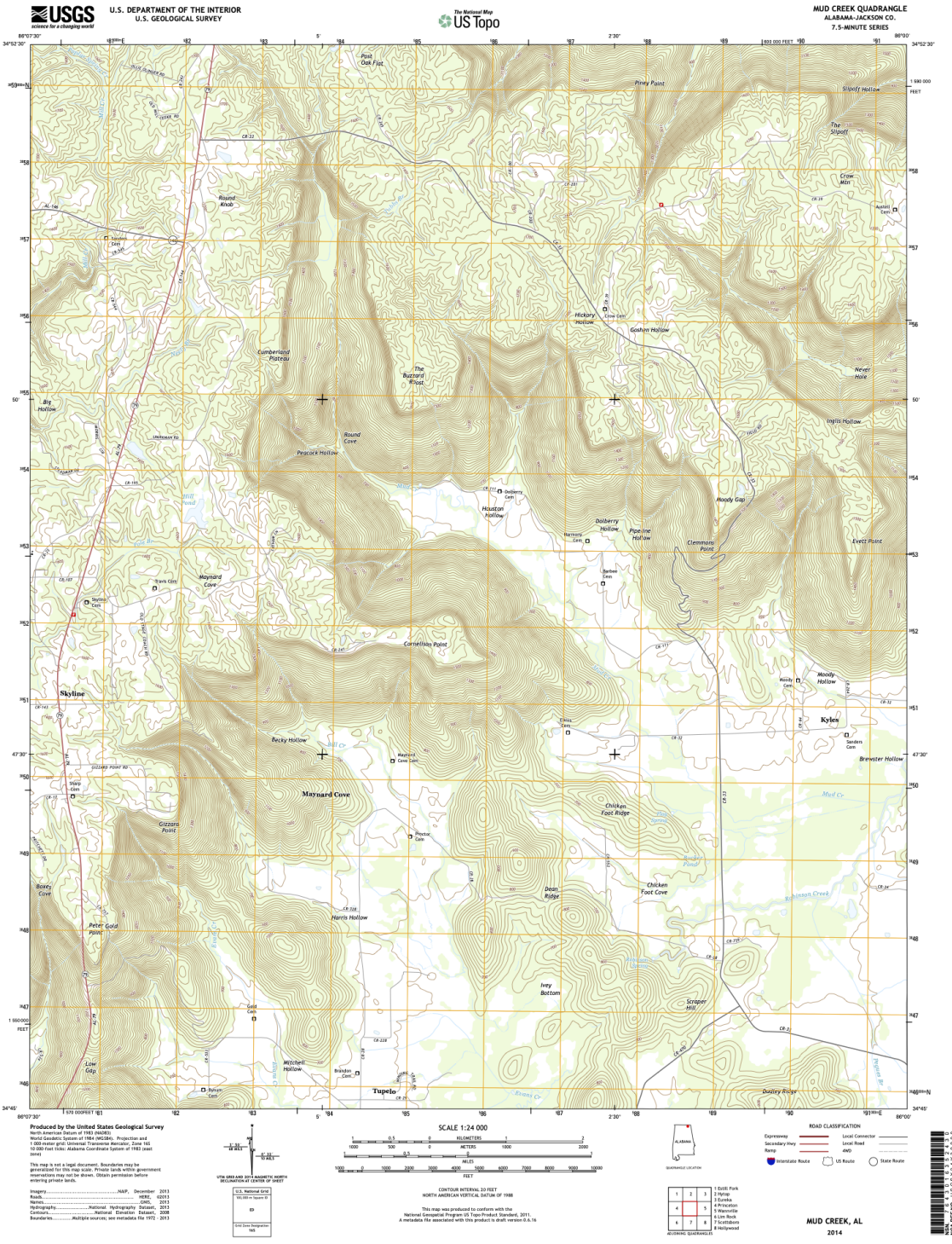

Figure 2.6: USGS topographic map, Mud Creek 7.5-min quadrangle, Jackson County, AL (USGS 2011).

Chapter 3

Methods

A number of methods and analyses are utilized in this study in order to understand and characterize the rock and water quality within the cave system. A number of laboratory tests and modeling will be used in order to accurately describe this karst system.

3.1 Field Procedures

3.1.1 Meteorology

Meteorological data is captured by a weather station installed roughly 60 m (200 ft) from the cave entrance. Precipitation, air temperature, wind direction, and speed are all collected using the weather station installed on the field site. Precipitation is recorded by the tipping bucket method. A tipping bucket funnels water into a calibrated "bucket" with a known volume that tips when it is full. This instrument measures the number of tips in a given time interval to determine the discharge of water. This instrument also measures air temperature and wind speed by use of an anemometer.

3.1.2 Streamflow

Water level (stage) and stream flow (discharge) data are measured at the resurgence (spring head) just outside of the cave entrance using a HOBO 13-Foot Water Level Data Logger and H-type flume which concentrates flow to a measurable point. Data is collected and stored on the HOBO sensor and retrieved monthly with a computer on-site. A nearby USGS stream gauge, Crow Creek, is used to compare with field measurements collected outside the cave.

3.1.3 Water Quality

The hydrology within the cave consists of one large stream passageway exiting at the cave entrance with multiple inputs from ceiling drips. The sampling consisted of 8 sites along the stream and 5 ceiling drips throughout the extent of sampling.

Water samples are collected from stream and drip sampling sites distributed throughout the length of the cave stream using whirl bags and analyzed for specific conductance (SpC), pH, total dissolved solids (TDS), and elemental concentrations. Sampling starts at the entrance of the cave labeled 1 and extends to the Topless Dome labeled 13 in Figure 3.1. SpC, pH, and TDS values are measured using a multi-probe (i.e., SpC, pH, temperature, TDS) in the Forest Hydrology Lab in Athens, GA. Calcium concentrations are measured using ICE 3000 series AAS (atomic absorption spectrometry) in the Crop and Soil Department. Elemental analysis tests are performed on thirteen water samples using Thermo X-Series II ICP-MS in the Crop and Soil Department.

3.2 Laboratory Procedures

Rock samples were extracted just outside the cave entrance. Due to the SCCi policies, no rock samples were taken from within the cave. The rocks outside the cave entrance appeared very similar to the Monteagle limestone within most of the cave.

3.2.1 Sample Preparation

Limestone samples are first washed with a coarse bristle sponge to remove any scum or debris on the surface. The Limestone samples are then cut into small fractions using a diamond-tipped rotary saw. The small fractions of rock are then crushed using a mortar and pestle until they pass through a 0.6096-cm sieve. The crushed and sieved material is then put in the oven at 230°C for four hours in order to sterilize and remove all moisture.

3.2.2 Leaching Study

A laboratory batch procedure for mineral weathering is performed to understand the kinetics of dissolution in a karst landscape. 250 g of the sieved rock material is added into an Erlenmeyer flask along with 500 mL of DI water. The Erlenmeyer flask is covered with para-film, and placed on a hot plate intended to reach a constant temperature of about 50-60°C for five days. The Parafilm has small holes to allow pressure exchange but limits the amount of moisture that can evaporate. Measurements and samples are taken daily at 12:00 pm. SpC, pH, TDS, and temperature are measured in situ. A 2 mL sample of supernatant is taken during each measurement and stored in a refrigerator between 1-4°C. The supernatant is then analyzed for calcium concentrations using an atomic adsorption spectroscopy (AAS) instrument.

3.2.3 X-Ray Diffraction Analysis

Limestone samples are cut and crushed with a similar methodology to the leaching study. For XRD preparation, the small fractions of rock are then crushed to a finer texture using a mortar and pestle until they are a fine powder. This is performed to accurately measure the shape, size, and orientation of the crystalline structure. The flour-like samples are placed between two small glass sheets before they are analyzed using an XRD instrument. The XRD instrument uses X-rays to identify the crystalline structure of the rock from the geometry of the crystals. The X-rays are then generated and detected through the sample. The XRD instrument then identifies the sample based on reference data for crystals and minerals.

3.2.4 Total Elemental Analysis (Acid Digestion)

Limestone samples are crushed into small fractions similar to that of the leaching and XRD sample preparation. Samples are placed in an oven at 45°C for 24 hours to dry. Samples are further crushed using a flail mill and passed through a 2 mm screen. The samples are then ready for digestion using EPA Method 3052 (USEPA, 1995). 1.00 g samples are placed

in polymer microwave vessels. 10 mL of concentrated HNO_3 are added to the vessels and sealed. The sample vessels are then placed in a digester at 200°C for 30 minutes. The digested samples are transferred to volumetric flasks and diluted with 100 mL of DI water. Using EPA Method 200.8 (Creed et al., 1994) the samples are analyzed using a Perkin Elmer 8300 ICP-OES at the Center for Applied Isotope Studies, UGA.

3.3 Geochemical Modeling - Excel/PHREEQC

Excel is used to extrapolate and predict the dissolution of calcite at various temperatures. Using equilibrium constants and reaction rates, we can predict the amount of dissolution over a certain period of time. In this study, we compare dissolution at 25°C and 65°C. This is done to observe the trends in dissolution in ppm and mmol/L between two temperatures based on theoretical constants.

Table 3.1 shows how a chemical reaction where reactants 'A' are converted into products 'B'. The rate of change between free calcium ions into saturated calcium is dictated by the reaction rate, the reactive surface area, solution volume, and time. In this study, we are interested in modeling 250 g of rock dissolved into 500 mL of DI water. 250 g of rock is sieved through a 0.0067 m screen. In order to estimate the surface area, we assume each rock fraction is a sphere, with a 15% porosity. From this, we determine a surface area of 0.1068 m^2 and a calcite solubility of 0.013 g/L at 25°C based on previous studies by Plummer 1978. Using this information we can predict the dissolution over time and observe how parameters affect the outcome of dissolution.

Table 3.1: Chemical reaction rate equations for calcite dissolution.

$A \rightarrow B$
$r = -\frac{dC_A}{dt} = \frac{dC_B}{dt}$
where r is a rate constant, C is solute concentration, and t is time
$\frac{dC}{dt} = \frac{k\,A}{V}(C_{sat} - C)$
where k is the reaction rate, A is the surface area, and V is the solution volume
$[Ca^{2+}]_t = [Ca^{2+}]_{sat}\,\left(1 - \exp\left(\frac{-k\,A\,t}{V}\right)\right)$
where $V = 0.5\text{L} = 0.0005\ \text{m}^3$, $A = 0.1068\ \text{m}^2$, and calcite solubility is 0.013 g/L at 25°C.

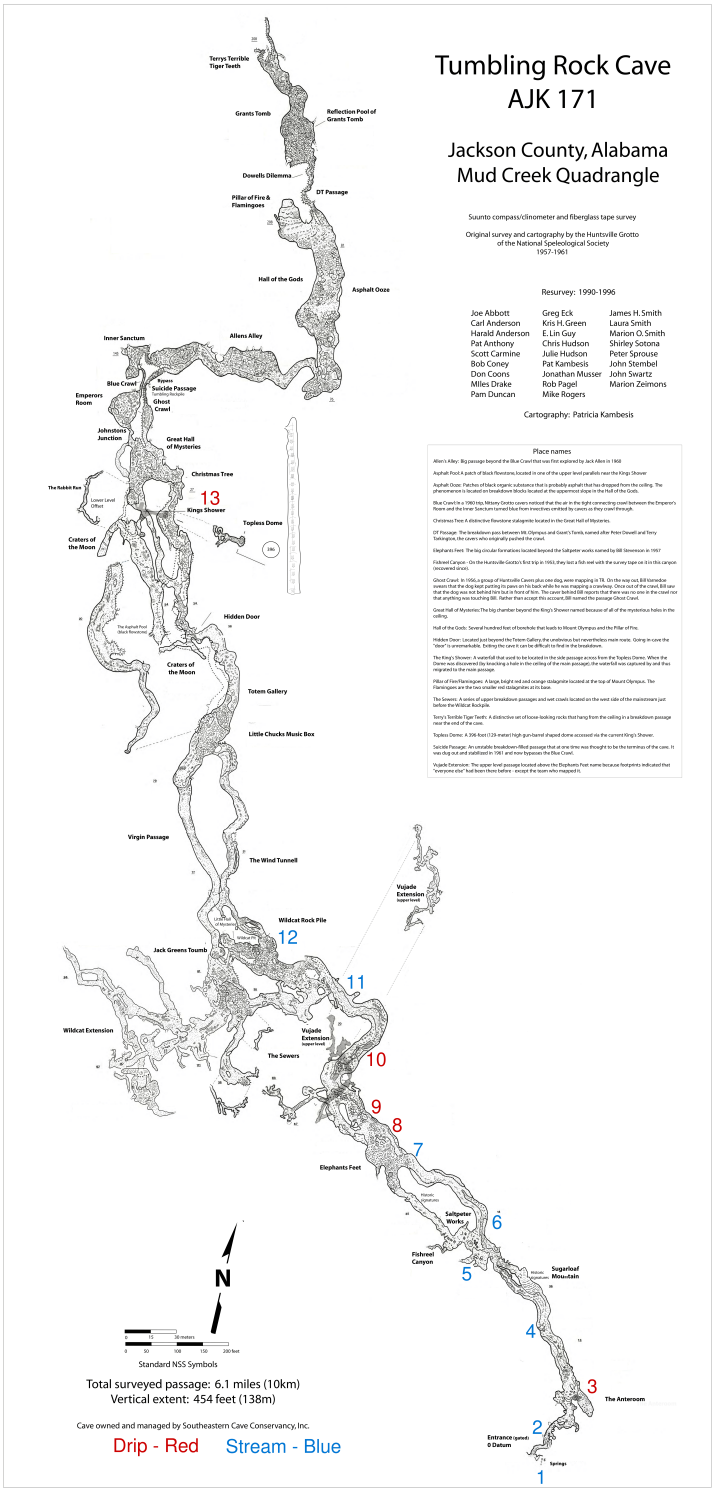

Figure 3.1: Map of Tumbling Rock Cave indicating the location of drip and stream sampling sites (modified from SSCi basemap)

Chapter 4

Results and Discussion

The purpose of this study is to identify the elemental composition of the water and minerals in Tumbling Rock Cave and understand the dynamics between them. Water quality sampling was able to identify the presence of elements and their relation with the surface and subsurface, while mineral sampling helps characterize the parent material of this karst system. The results of the study confirm that there are a number of factors that contribute to the dissolution of carbonate rock. The pH, temperature, and the presence of other elements seem to have the largest influence on the rates of dissolution.

4.1 Hydrology

Surface hydrology is crucial in karst landscapes as it is responsible for the quantity of water interacting with the rock and chemically responsible for controlling parameters of dissolution. The Southeast United States typically receives significant amounts of rainfall compared to the rest of the country in any given year. The amount of rainfall and quality of the water play a large role in the amount of dissolution that occurs in this region.

Figure 4.1 shows the cumulative precipitation in a 5-month period (November 2022 through March 2023) outside the cave entrance totaled just under 75 cm (30 in) of rain. This amount of rain leads to a substantial amount of surface flow, recharge, and groundwater flow. The discharge at the cave, shown in Figure 4.2, identifies spikes in water level and stream flow during these precipitation events.

For example, we observed a large precipitation event (12 cm) in early December of 2022 followed by a large response in both stage and discharge. The stage and discharge are measured at the springhead of the cave, so while it has some inputs from surficial flow, a large percentage of the flow is coming from the groundwater within the cave. To evaluate the trends in discharge we observe at the cave, a USGS stream gauge (Crow Creek) is used for comparison shown in Figure 4.3.

When comparing precipitation to flow at the resurgence and Crow Creek, Figure 4.4, we see very similar spikes in discharge due to these precipitation responses. This confirms the trends in flow we observe at the cave. During large precipitation events, runoff is able to transport a large quantity of inorganics and organics, some of which are responsible for the dissolution of the parent material. During recharge events, many of these ions infiltrate the groundwater through soil, losing streams, and sinkholes. These ions, especially carbon, lead to water quality that is susceptible to dissolving the rock. This cycle is especially important during large precipitation events when runoff on the surface and flooding within the cave increases.

4.2 Rock and Mineral Composition

Characterizing the rock composition is vital in understanding chemical processes in the cave. In this study, we characterize the rock with the use of Acid Digestion and XRD. Acid Digestion of the rock shows the elemental composition of the rock, whereas XRD gives insight into the mineralogy of primary and secondary minerals present. Understanding the elemental composition can help us predict what ions should dissolve or precipitate based on the conditions.

4.2.1 Total Elemental Analysis (Acid Digestion)

The acid digestion analysis revealed 18 elements within the rock samples. Of the 18, only six major elements (Al, Ca, Fe, K, Mg, and S) had values of magnitude greater than [500ppm],

shown in Table 4.1. Calcium presented the greatest concentration (97.3%) of the elements analyzed in the acid digestion procedure. This is expected as TRC is thought to be predominately made of calcium carbonate. Limestone is a significant geologic feature in karst landscapes and in Northeast Alabama, which is abundant in Limestone. High calcium concentrations in the mineral samples are the first suggestive characteristic of karst regions.

The other major elements from the acid digestion test are shown in Table 4.2. Sulfur was the second-greatest concentration of any element (0.88%). Although significantly lower than the calcium concentration, the presence of sulfur can play a large role in dissolution. As sulfur is introduced to the water matrix, it can form sulfuric acid which further lowers the pH and enhances the dissolution of calcite minerals. Aluminum accounts for 0.34% of elements but is the first indication that aluminum silicates could be present in the cave. Aluminum is common in micas (muscovite) and clays (kaolinite). Magnesium and potassium accounted for 0.82% and 0.20% respectively of the total elements identified. The presence of magnesium and potassium in the mineral samples is another indicator that the formation of micas and clays is possible. Finally, Iron accounted for 0.33% of the analyzed material. Similar to sulfur, iron can become a problem with acidic water especially if pyrite ($Fe_{2+}S$) is present in the bedrock.

This is commonly a problem on mine sites with exposed waste rock piles. Sulfur and iron can become oxidized, especially with the help of bacteria, during pyrite oxidation leading to acidic discharge (Taylor et al., 1984). This usually occurs at a smaller scale in a cave, unless the presence of pyrite is abundant similar to that of a mine site.

All of these elements help elucidate the geologic history of TRC and introduce the possibility for a variety of deposition events whether through parent rock weathering or surficial input from subsurface flow. The presence of these elements also gives some insight into their influence on environmental conditions such as pH, EC, TDS, and other water quality parameters.

4.2.2 X-Ray Diffraction Analysis

XRD was performed on two different rock fractions collected from outside the cave entrance. Information provided by the SCCi and other scientists who have explored the cave indicated the presence of Monteagle and Bangor limestone within and adjacent to the cave. The collected samples visually showed qualities of limestone and sandstone. The XRD analysis was done in order to verify this and to determine and quantify the minerals within the rock shown in Table 4.3 The XRD software was then able to identify peak positions, intensities, and widths in order to identify the crystalline structure.

At the Department of Geology, UGA, using the Bruker D8-Advance X-Ray Diffraction instrument. XRD is performed on two fractions of the rock, the matrix (1) and the weathered surface (2) as shown in Figure 4.5. The matrix is more analogous to the parent material of the cave while the weathered surface is indicative of fractures and conduits. The matrix analysis revealed peaks for 89% calcite, 10.8% mica/muscovite, and 0.2% quartz shown in Figure 4.6. This high percentage of calcite is expected for a limestone sample. The weathered surface shows evidence of dissolution with the introduction of kaolinite, a clay mineral, shown in Figure 4.7. We found that the XRD of the weathered surface had peak values of 68.6% calcite, 16.8% mica, 11.7% kaolinite, and 2.9% quartz. The chemical reaction from Mica to Kaolinite is anticipated as the Mica becomes exposed to meteoric water. In the matrix, these minerals are less exposed to air, water, and transport than on the weathered surface. The weathered surface represents a preferential flow path where a fracture or conduit could occur. As the Mica is exposed to the meteoric water it is able to seemingly leave behind more silicate minerals (Mica and Muscovite) on the weathered surface. Kaolinite forms from most aluminum silicate minerals, found in muscovite and quartz. Figure 4.8 shows the difference between two weathered rocks found in the cave, mostly calcite mineral (left) versus a calcite mineral with low porosity used in this study (right).

4.3 Water Quality

The quality of water, surface or groundwater, is important from ecological and geochemical standpoints. Globally karst regions lack sufficient surface water resources for at least part or all of the year. These areas rely on groundwater for drinking water, irrigation, and manufacturing. Typically, groundwater is potable, where minimal, if any, purification is required for usage. Most private homes lack water filtration or treatment systems. This is one of many reasons why water quality is important in groundwater. Groundwater in karst regions is susceptible to contamination because of the lack of surface water and rapid recharge. Understanding the water quality of karst regions is vital as most of the global population lives in these regions.

Geochemically, water quality dictates the minerals present and the amount of dissolution the parent material is susceptible to. Understanding the different parameters of water quality, pre and post-dissolution allows us to predict and interpret the chemical reactions underway. From an ecological standpoint, water quality is important to an ecosystem as it serves as a home for aquatic organisms, provides nutrients to plant life, and supplies all other wildlife.

Water quality sampling consisted of 13 sampling sites, 12 within the cave and one at the resurgence. These samples were tested for pH, conductivity, TDS, and elemental concentrations. The purpose of this sampling was to compare the similarities and differences between stream and drip samples. In this section, we are more concerned about observing similarities and differences between the trends of stream and drips. Because these values are measured ex-situ we are more interested in ranking and trends between the observations. Stream samples tended to have lower pH, TDS, and calcium concentrations than drip samples. Table 4.4 shows the breadth of the cave study water quality. From this table, we observe greater pH in the stream samples and greater specific conductance, TDS, and Ca^{2+} in the drip samples. Generally, all stream and drip values behaved similarly to their sample group with the exception of Sample 6. Sample 6 was taken out of the stream about halfway through the

length of this cave study. This section of the stream tends to disappear and reappear which may have other inputs that are not immediately visible. Because of this, Sample 6 tends to respond more like a drip sample than a stream sample.

In Figure 4.9, we observe greater specific conductance in the drip samples with the largest value in Sample 13, the Topless Dome feature. Cave drips interact with the minerals of the cave more directly than stream samples. This leads to increased dissolution within the drips causing more dissolved ions, thus increasing specific conductance. Cave drips likely see more influence from surface water, which can introduce other ions brought in from human and wildlife influence on the surface. This would likely explain why Sample 13, which has been known to see a quicker response to surface precipitation, had the greatest specific conductance. The stream is likely more dilute than the drip samples because of the multiple sources and volume of water. This leads the stream samples to have a lower specific conductance.

In Figure 4.10, we observe higher TDS in the drip samples compared to the stream samples. We observe similar trends to that of the specific conductance, with stream Sample 6 behaving like a drip sample. We would expect to see similar trends between each of these water quality parameters. TDS is a measure of the amount of organic and inorganic material dissolved in the water, while specific conductance is measuring the concentration of ions in the water that have the ability to conduct electricity. Because of this, we can validate the results between EC and TDS. We also expect these TDS values as the drip samples are exposed to more dissolution and surface inputs.

The pH of water is a commonly used water quality measurement and can be the first indicator of water quality problems. In this karst system, pH is used to differentiate the stream and drip sites. In Figure 4.11, we see that pH is greater in the stream samples than in the drip samples. This could be caused by the production of carbonic acid in the drips driving the dissolution. As the rain water percolates through the soil and accumulates carbon dioxide from the organic material and forms carbonic acid leading to a slightly lower pH. As the

water breaks down the mineral, more Ca^{2+} ions are introduced and accumulate in the stream increasing the pH further down the cycle. The acidic water plays a large role in the dissolution of limestone. Another reason for lower pH in the drips could be caused by the dissolution of limestone releasing ions other than calcium such as sulfur or iron thus increasing dissolution further along the flow cycle. As the waters reach the stream it becomes dilute as shown in the previous figures for SpC, TDS, and calcium concentrations.

4.3.1 Atomic Absorption

Table 4.5 shows water samples analyzed through the atomic absorption spectroscopy instrument. Identified trends in the cave sampling throughout the drips and stream as well as the leaching study. The AA was performed on 18 different water samples. Samples 1-13 are from the cave site, while samples 14-18 are from Days 1-5 in the leaching study.

As water in the subsurface interacts with carbonate minerals, such as limestone, calcium ions are released. Environmental conditions such as pH, temperature, and elements in the water drive the speed of this reaction. High concentrations of calcium in natural waters can be indicative leaching of carbonate rocks. Figure 4.12 shows calcium concentrations were greater in the drip samples compared to the stream samples. Drips are much higher in calcium due to fracture and matrix flow directly on the rock surface. The drip flows are what contribute the most to dissolution over time. As the water flows into the main stream channel mixing caused the calcium concentrations to become dilute. Calcium concentrations and pH were the water quality parameters of most interest. Similar to that of SpC and TDS, we expect higher calcium in the drip samples as this is where the most dissolution occurs.

4.3.2 ICP

A non-targeted ICP analysis was performed on the 13 water samples in order to identify the major ions within the water. The first ICP tested for 29 different ions at a dilution of 1:100 and only identified relevant concentrations for Na, Mg, K, and Ca. The ICP was rerun

testing for only 11 ions that were previously detected, at a dilution of 1:1000, to validate negligible concentrations. Elements besides Na, Mg, K, and Ca were still negligible. Table 4.6 shows the concentrations for Na, Mg, K, and Ca adjusted for their stable isotope based on the percentage of each isotope analyzed. As expected, calcium concentrations were the highest of any ion identified, because of its large value, Table 4.7 shows the log values for ICP results. Figure 4.13 shows the Log ICP data for the four major cations identified within the cave samples. The stream samples identified higher concentrations for Na, Mg, and K, while the drip samples were higher in Ca. We believe dissolution is occurring within the drip samples, we would expect higher concentrations of calcium as previously identified in the AA results. Because the stream has inputs from multiple drips and lateral groundwater flow, it would make sense that these samples were greater in elements other than calcium.

Overall, we observed higher concentrations of calcium within the drip samples and lower pH. Because of this, we believe that more dissolution is occurring within the drips. More dissolution could be indicative of longer water and rock interactions leading to longer residence time. This is important in a karst system as it could be a sign that this system is less susceptible to pollution and contamination due the the increased residence times. This is consistent with contamination and residence time hypotheses between the conduits (rapid flow) and drips (slow flow) shown by Normile 2022.

4.4 Laboratory Procedures

In order to make predictions about surface-groundwater interactions, a leaching study is performed to simulate dissolution within the cave. This leaching study is meant to expedite the chemical reactions occurring by controlling the temperature and concentration of calcite. Geochemical modeling provides another predictive approach to the reactions.

4.4.1 Leaching Study

To understand dissolution in the cave, a laboratory leaching study was set up using carbonate samples. Over the course of 5 days, 250 g of crushed minerals were dissolved in 500 mL of DI water in order to track changes in pH, conductivity, total dissolved solids, and calcium concentrations. The mineral water slurry was heated to roughly 65°C over the five-day period to enhance the dissolution rate. Table 4.8 shows the parameters of the leaching study over the duration of the experiment. The goal of the experiment was to control the temperature at 65°C, although the initial temperature conditions barely broke 20°C and took two days to exceed 60°C. Many experimental issues can arise when using a hot plate, such as human error, electrical problems, or faulty equipment. Because of these issues, maintaining a constant temperature can be difficult to maintain. Another potential issue with this setup was the solution evaporating over time. To minimize evaporation, the beaker was covered with Parafilm and pierced with a few small holes to allow some air/water to escape. The weight of the beaker and sample was recorded over the experiment, which had decreased by 33 g over five days.

The pH of the sample became more acidic over the course of the experiment. After the first day, the pH was 9.74, which is likely due to the initial powder from the crushed mineral immediately dissolving into the DI water. The pH declined over the experiment to 8.37 by the final sample. Figure 4.14 shows the inverse relationship between pH and calcium concentrations in this batch sample with the solubility of calcium carbonate at 25°C (1.3 mg/L) and 65°C (11 mg/L). The addition of calcium typically raises the pH as it replaces free hydrogen ions. In this experiment as the calcium concentrations increased the pH decreased. This could be due to the influence of other mineral elements dissolving in the water or an increase in carbon dioxide. Carbon dioxide dissolving in water can form carbonic acid, which assists in speeding up dissolution while lowering the pH.

As more ions are introduced to the water the TDS and SpC should increase as a result. There is a directly proportional relationship between SpC and TDS shown in Figure 4.15. This is expected as more of the mineral is dissolved, the TDS should increase and the presence of ions should increase. In this experiment, we observe how lower temperatures cause more dissolution than higher temperatures. The slowing of dissolution is likely due to the increased temperature of the solution, but could also be representative of the reaction approaching equilibrium.

4.5 Geochemical Modeling

Geochemical modeling is critical in predicting mineral dissolution, understanding equilibrium kinetics, and characterizing a geologic environment, especially a karst environment. Geochemical modeling can be utilized to validate field and laboratory analyses but is typically used for predictive testing. In mining, understanding mineral dissolution is very important in cost-effective yield and minimizing costly environmental impacts. In this study, geochemical modeling is used in order to understand the processes in the cave and how they compare to field and laboratory data. Using values from literature and PHREEQC on calcite dissolution we are able to describe the geochemical reactions.

Calcium equilibrium kinetics describes the expected rates of dissolution due to environmental factors that influence the rates such as temperature, pH, pressure, and concentration. The solubility describes how easily a substance can dissolve in a solvent (Johnson, 2004). The equilibrium constant describes a point at which the reaction is neither precipitating nor dissolving. Once a reaction reaches chemical equilibrium, the direction of the equation can shift in either direction, precipitating or dissolving calcium carbonate, known as Le Chatelier's Principle. This is closely related to the solubility, once the equilibrium has been surpassed the reaction will change from dissolution to precipitation. In this study, we assume atmospheric pressure and an initial pH of 7 and aim to investigate changes in the temperature

and surface area-volume ratio of the sample. As the temperature and surface-area volume ratio are manipulated we observe notable changes in the solubility and the kinetics.

We determined the kinetics of dissolution and equilibrium constants at various temperatures (Garing, personal communication, based on Plummer, 1978; Appelo and Postma, 2004; Morse and Arvidson, 2002; Pokrovsky et al., 2009). Note that the solubility of calcite decreases with temperature (Table 4.9) while the kinetics of dissolution increases with temperature (Table 4.10), based on previous experimental studies on calcite dissolution (Garing, personal communication). We observe an almost linear relationship between these in Figures 4.16 and 4.17.

Geochemical modeling was performed to understand dissolution occurring in the leaching study and make predictions about chemical reactions occurring within the cave. We first determine the total reactive surface area of the batch sample. Table 4.11 describes a batch sample using the same variables as the leaching study. In this batch reaction, 250 g of mineral is "dissolved" in 500 g (mL) of DI water. To calculate the total reactive surface area, we first characterize the average size, volume, porosity, and weight of each mineral fraction. All fractions were first sieved through a 0.61 cm diameter screen. The surface area of each fraction was determined assuming a spherical shape. We assume a 15% porosity and a density of 2.71 g/cm^3 for calcite based on the literature. From this, we determine a total reactive surface area of 0.106 m^2 per sphere. Roughly 915 individual spheres are determined based on the total sample weight and weight of each sphere shown in Table 4.11. The reactive surface area is important in dissolution as it dictates the amount of available space for chemical reactions, the smaller the fractions the more available surface area. In this batch reaction, we observe a large total value for the exposed surface area due to the size of the mineral fractions that were fragmented.

To compare different ratios of surface area and volume, three theoretical samples are compared to the batch sample. Table 4.12 compares three theoretical samples with different

volumes and surface area-volume ratios to the batch sample. The diameters of each of the three theoretical samples are 0.10, 0.02, and .01 m respectively, and are dissolved in 1 L of water. From this table, we can observe the surface area increases as the diameter of the mineral decreases. The same is true for the surface area-volume ratio with respect to diameter size. Based on the surface-area volume ratio we can now determine the rate of dissolution. Table 4.13 identifies the reaction rate and concentration equilibrium for the batch reaction at 25°C and 65°C. As previously described, the reaction rate is greater at lower temperatures due to the solubility and equilibrium constant. Using the equilibrium constants and reactions previously described, we can now incorporate the reactive surface area to estimate calcite dissolution at different temperatures.

$$A \rightarrow B \tag{4.1}$$

$$[Ca^{2+}]_t = [Ca^{2+}]_{sat} \left(1 - \exp\left(\frac{-k\,A\,t}{V}\right)\right) \tag{4.2}$$

where $V = 0.5\text{L} = 0.0005$ m^3, $A = 0.1068$ m^2, and calcite solubility is 0.013 g/L at 25°C.

Using the equation above we are able to model calcite dissolution, by predicting the concentration of calcium per time. In this reaction, "$[Ca^{2+}]_{sat}$" = calcium equilibrium, "k" = reaction rate constant, "A" = surface area of mineral, "V" = volume of solution and "t" = time.

Figure 4.18 shows the dissolution of calcium (mmol/L) at 25°C over 100 days. From this figure, we observe a linear relationship when the area-volume ratio is lower, and more of a non-linear relationship for higher area-volume ratios. We observe these dissolution curves decreasing at higher area-volume ratios compared to the lower ratios. Figure 4.19, shows the same dissolution temperature, but in ppm, over the course of ten days. In Figure 4.19, the dissolution curves show more of a linear relationship.

We next observe the dissolution trends for the same area-volume values but at 65°C. As expected, we observe lower dissolution at higher temperatures but similar trends and responses between ratios, shown in Figure 4.20 and 4.21.

The temperature of the reaction at 25°C and 65°C were chosen based on the results shown in the laboratory leaching study. The leaching study had an initial temperature of about 25°C and a final temperature at about 65°C. We do not observe the exact responses in the leaching study as we do in the geochemical modeling but observe similar plateauing occurring after 5 days of leaching, although the values in the leaching study are much greater than the modeling shows. This could be due to an initial spike of calcium dissolving into the solution and then slowly dissolving over the course of a few days.

The rock-water interactions shown in Figures 4.18, 4.19, 4.20, and 4.21 are based on theoretical calculations and give insight into the trends between temperature and particle size. We are able to determine that more dissolution is expected at lower temperatures due to the calcite kinetics. We also see that smaller particle size increases expected dissolution. Particles interacting with water within a cave system are dependent on the porosity of the mineral. These theoretical calculations allow us to consider how things may behave within TRC based on temperatures and reactive surface area within the cave. The batch experiment is likely more accurate in demonstrating dissolution than the modeling but is more difficult to reproduce. In the batch experiment, we are able to calculate dissolution reaction rates, whereas the modeling uses calculations and previous studies to determine reaction rates at 25°C and 65°C.

Calcite dissolution within the cave likely behaves differently than the theoretical and batch samples shown in this study. Temperature within the cave should be roughly 10-15°C, and fluctuate based on the depth and position within the cave. Lower temperatures expected within the cave will increase the concentration equilibrium and decrease the dissolution rates. Greater temperatures were used in the batch study based on previous experiments

performed by Plummer (1978), Appelo and Postma (2004), Morse and Arvidson (2002), and Pokrovsky et al. (2009).

The dissolution kinetics used in this modeling assume atmospheric pressure. Pressure within the cave is assumed to be at, or near, atmospheric pressure but could fluctuate based on depth and position in the cave. With changes in pressure, we would expect different CO_2 concentrations, altering the dynamics of calcite dissolution. Lastly, flow within the cave would change the behavior of dissolution. Slow (fracture-drip) subsurface transport would invite more dissolution with longer water-rock interactions, while rapid (channel-conduit) subsurface transport will introduce greater volumes of water, over shorter residence times.

Table 4.1: ICP-OES results from acid digestion (mg/L) of three samples using nitric acid.

Element	Sample				
	1	2	3	Mean	Std dev
Al	1,234.00	1,070.00	1,083.00	1,129.00	91.16
As	1.39	0.99	0.41	0.93	0.49
B	4.73	4.29	4.41	4.48	0.23
Ca	325,532	319,368	319,951	321,617	3,403.00
Cd	0.39	0.43	0.40	0.41	0.02
Cr	8.96	6.54	5.93	7.14	1.60
Cu	9.09	7.34	7.85	8.09	0.90
Fe	1,161.00	1,078.00	1,026.00	1,088.33	68.09
K	726.00	647.00	652.00	675.00	44.24
Mg	2,687.00	2,733.00	2,686.00	2,702.00	26.85
Mn	43.20	41.70	40.10	41.67	1.55
Mo	0.65	0.27	0.21	0.38	0.24
Na	172.00	171.00	170.00	171.00	1.00
Ni	4.59	3.58	3.33	3.83	0.67
P	62.40	60.10	60.90	61.13	1.17
Pb	1.63	2.04	1.27	1.65	0.39
S	2,897.00	2,914.00	2,892.00	2,901.00	11.53
Zn	129.00	107.00	104.00	113.33	13.65

Table 4.2: Major elements identified from acid digestion analysis.

Element	Average	
	(mg/L)	(Percent)
Al	1,129	0.34%
Ca	321,617	97.30%
Fe	1,088	0.33%
K	675	0.20%
Mg	2,702	0.82%
S	2,901	0.88%
All Other Elements	414	0.13%

Table 4.3: Crystalline structures identified from XRD analysis of rock matrix and weathered surface.

Mineral	Matrix	Weathered Surface
Calcite	0.89	0.686
Mica/Muscovite	.018	.168
Kaolinite		.117
Quartz	.002	.029
Total	100%	100%

Table 4.4: Water quality parameters for thirteen water samples (drips and streams) within Tumbling Rock Cave.

Sample	Type	pH	SpC (μS/cm)	TDS (mg/L)	Ca^{2+} (mg/L)
1	Stream	9.67	128.7	93.2	11.571
2	Stream	9.82	126.6	93.4	8.569
3	Drip	9.16	133.1	101	22.523
4	Stream	9.94	122.0	88.7	6.035
5	Stream	10.22	118.1	85.6	3.1
6	Stream	9.14	136.4	105	20.63
7	Stream	10.05	121.1	88.1	4.823
8	Drip	9.13	134.1	102	11.005
9	Drip	9.50	135.4	104	6.86
10	Drip	9.46	127.5	93.6	5.855
11	Stream	10.03	121.2	88.5	3.992
12	Stream	10.26	123.5	91.1	3.466
13	Drip	8.17	152.7	118.0	12.25
Average	Stream	9.89	124.77	91.7	7.77
	Drip	9.084	136.56	103.72	11.69

Table 4.5: Atomic absorption results from thirteen water samples collected within Tumbling Rock Cave (Samples 1-13) and five laboratory leaching study samples (Samples 15-18). D = drips, S = streams

Correlation Coefficient	0.977374
Slope	0.05993
intercept	0

Sample	ID	Calcium (mg/L)
Cave Water Samples	1S	11.571
	2S	8.569
	3D	22.523
	4S	6.035
	5S	3.1
	6S	20.63
	7S	4.823
	8D	11.005
	9D	6.86
	10D	5.855
	11S	3.992
	12S	3.466
	13D	12.25
Leaching Study	Day	
	1	10.476
	2	18.757
	3	18.436
	4	18.383
	5	13.405

Table 4.6: ICP results adjusted for stable isotope for the major cations identified from 13 water samples (drip and stream) within Tumbling Rock Cave (ppb) - Sampled and analyzed February 2023.

Sample	Drip/Stream	^{23}Na	^{24}Mg	^{39}K	^{43}Ca
1	Stream	2,142.7	59.4	526.7	111,333.3
2	Stream	3,953.6	64.9	22.8	87,259.3
3	Drip	2,860.9	60.9	11.0	248,592.6
4	Stream	3,107.4	35.3	13.4	72,814.8
5	Stream	3,688.9	36.7	86.5	69,629.6
6	Stream	2,878.8	67.8	57.7	150,963.0
7	Stream	3,718.0	41.0	286.8	3,333.3
8	Drip	4,417.8	52.3	17.5	100,074.1
9	Drip	4,030.2	41.5	33.8	82,814.8
10	Drip	4,526.1	32.7	56.8	11,185.2
11	Stream	3,881.3	36.5	48.6	65,037.0
12	Stream	5,017.8	36.2	85.4	56,370.4
13	Drip	24.9	31.5	35.8	90,666.7
Average	Stream	3,154.28	41.978	125.322	68,526.74
	Drip	2,266.76	37.24	19.62	104,429.64

Table 4.7: Log-ICP results for major cations Identified from 13 water samples (drip and stream) within Tumbling Rock Cave - Sampled and analyzed February 2023.

Sample	Drip/Stream	Log ^{23}Na	Log ^{24}Mg	Log ^{39}K	Log ^{43}Ca
1	Stream	3.3310	1.7735	2.7216	5.0466
2	Stream	3.5970	1.8125	1.3585	4.9408
3	Drip	3.4565	1.7845	1.0430	5.3955
4	Stream	3.4924	1.5480	1.1270	4.8622
5	Stream	3.5669	1.5648	1.9370	4.8428
6	Stream	3.4592	1.8315	1.7609	5.1789
7	Stream	3.5703	1.6129	2.4576	3.5229
8	Drip	3.6452	1.7183	1.2423	5.0003
9	Drip	3.6053	1.6182	1.5284	4.9181
10	Drip	3.6557	1.5140	1.7544	4.0486
11	Stream	3.5890	1.5618	1.6862	4.8132
12	Stream	3.7005	1.5587	1.9316	4.7510
13	Drip	1.3962	1.4986	1.5539	4.9574
Average	Stream	3.4988	1.62304	2.0980	4.8358
	Drip	3.3554	1.5710	1.29263	5.0188

Table 4.8: Water quality parameters, temperature, and beaker mass during a five-day leaching study - February 6-10, 2023

Day	pH	SpC (μS/cm)	TDS (mg/L)	Ca^{2+} (mg/L)	Temp (°C)	Mass (g)
1	9.74	62.2	43.1	10.476	20.2	1473
2	9.18	88.8	64.4	13.405	46.3	1468
3	8.31	152.4	110	18.757	62.5	1462
4	8.41	154.1	114	18.436	63.1	1452
5	8.37	183.5	122	18.383	63.5	1440

Table 4.9: Calcium equilibrium kinetics at temperatures ranging from 10-70°

Temp (°C)	Ca^{2+} eq (mmol/L)
10	0.6211
15	0.5722
25	0.4828
30	0.4423
40	0.3698
50	0.3080
60	0.2565
65	0.21105
70	0.1656

Table 4.10: Kinetics for dissolution at temperatures ranging from 2.5-70°

Temp	k		r	aH	
(°C)	(cm/s)	(m/s)	(mmol/m^2/s)	(mmol/L)	(mmol/m^3)
2.5	0.039	0.00039	1.00E-06	2.56E-06	2.56E-03
11.5	0.043	0.00043	1.05E-06	2.43E-06	2.43E-03
25	0.051	0.00051	1.11E-06	2.17E-06	2.17E-03
34	0.057	0.00057	1.14E-06	2.00E-06	2.00E-03
45	0.068	0.00068	1.18E-06	1.73E-06	1.73E-09
55	0.071	0.00071	1.02E-06	1.44E-06	1.44E-03
65	0.073	0.00073	8.18E-07	1.12E-06	1.12E-03
70	0.075	0.00075	7.20E-07	9.60E-07	9.60E-04

Table 4.11: Theoretical batch reaction identifying sample mass, volume, and total reactive surface area

DI water	500	(g)
Sample weight	250	(g)
Sieve diameter	0.6096	(cm)
Sieve radius	0.3048	(cm)
Sieve radius	0.003048	(m)
Surface area (sphere)	0.00011668622	(m^2)
Volume (sphere)	1.19E-07	(m^3)
Volume at 15% porosity	1.01E-07	(m^3)
Grain density of calcite	2.71	(g/cm^3)
Volume	0.100770218	(cm^3)
Sphere weight	0.273087291	(g)
Number of spheres	915.4582006	
Total reactive surface area	0.106821355	(m^2)

Table 4.12: Surface area and volume ratios of based on diameter of mineral

Theoretical Sample		1	2	3	Batch
Sieve Diameter	(m)	0.1	0.02	0.01	0.0067
Area	(m^2)	0.0126	0.063	0.126	0.10682136
Volume	(L)	1	1	1	0.5
Volume	(m^3)	0.001	0.001	0.001	0.0005
Ratio (A/V)	(m)	12.6	63	126	213.642711

Table 4.13: Reaction Rate and Equilibrium Constant 25° and 65° at Atm Pressure for Batch Sample

Temperature (°C)	Reaction Rate, k (mmol/m2/s)	$[Ca^{2+}]$ eq (mmol/L)
25	0.00000339	0.4828
65	0.00000485	0.21105

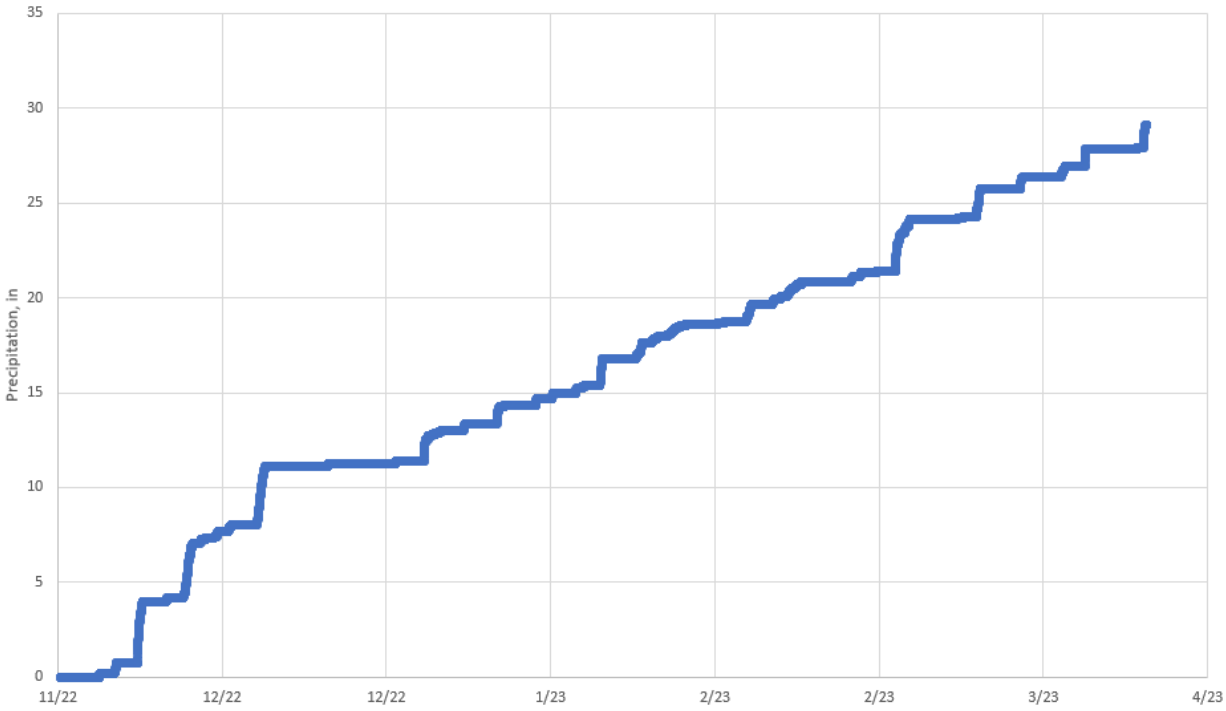

Figure 4.1: Cumulative precipitation (in) at Tumbling Rock Cave entrance - Nov 2022 to Apr 2023.

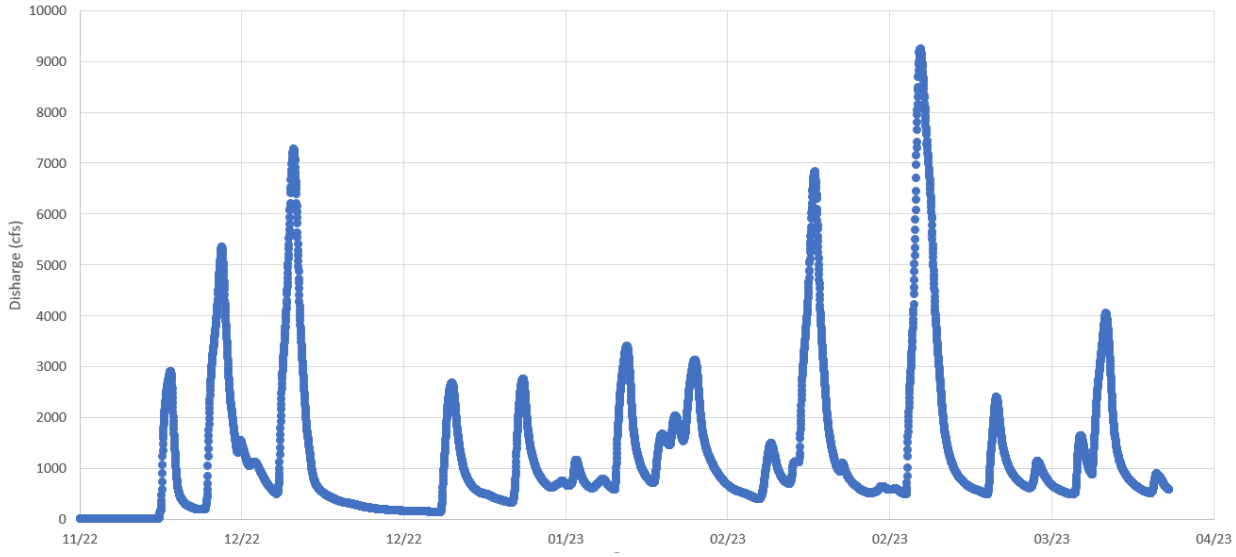

Figure 4.2: Spring discharge (cfs) at Tumbling Rock Cave entrance - Nov 2022 to Apr 2023.

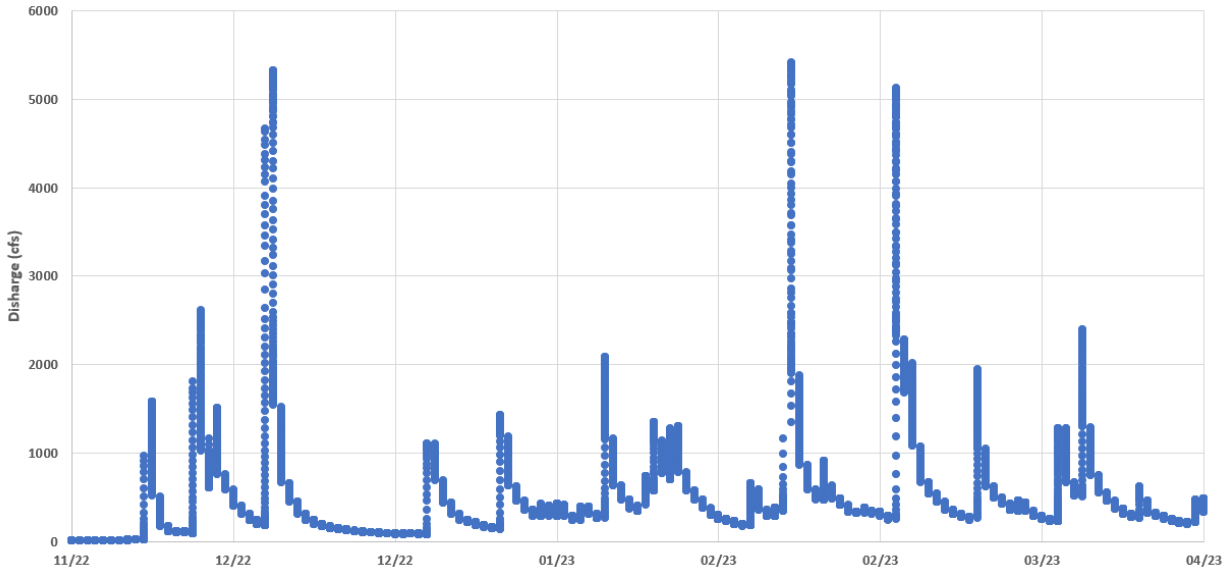

Figure 4.3: Discharge (cfs) at Crow Creek at Bass, AL (USGS 03572110) - Nov 2022 to Apr 2023.

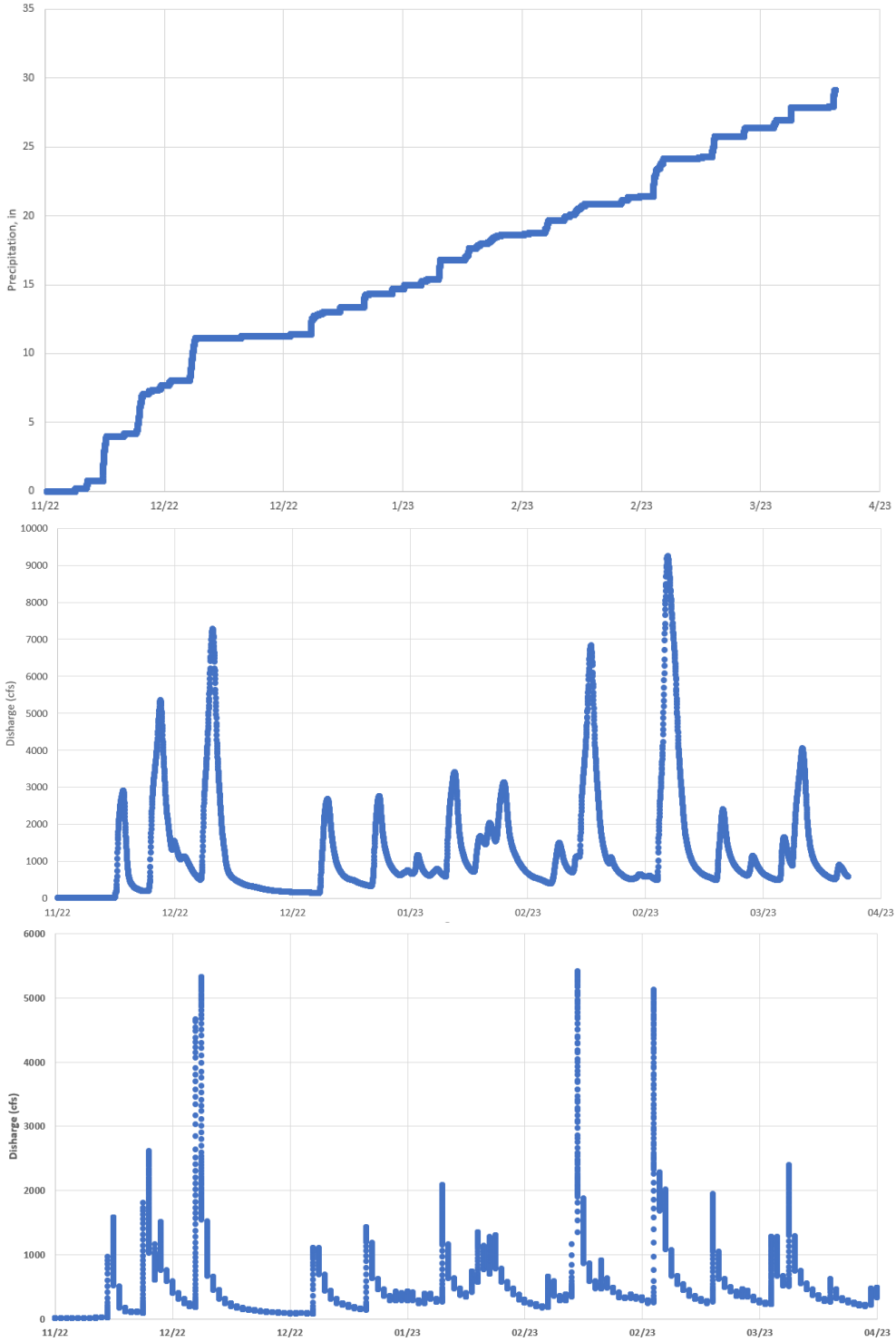

Figure 4.4: Site precipitation and discharge - Nov 2022 to Apr 2023

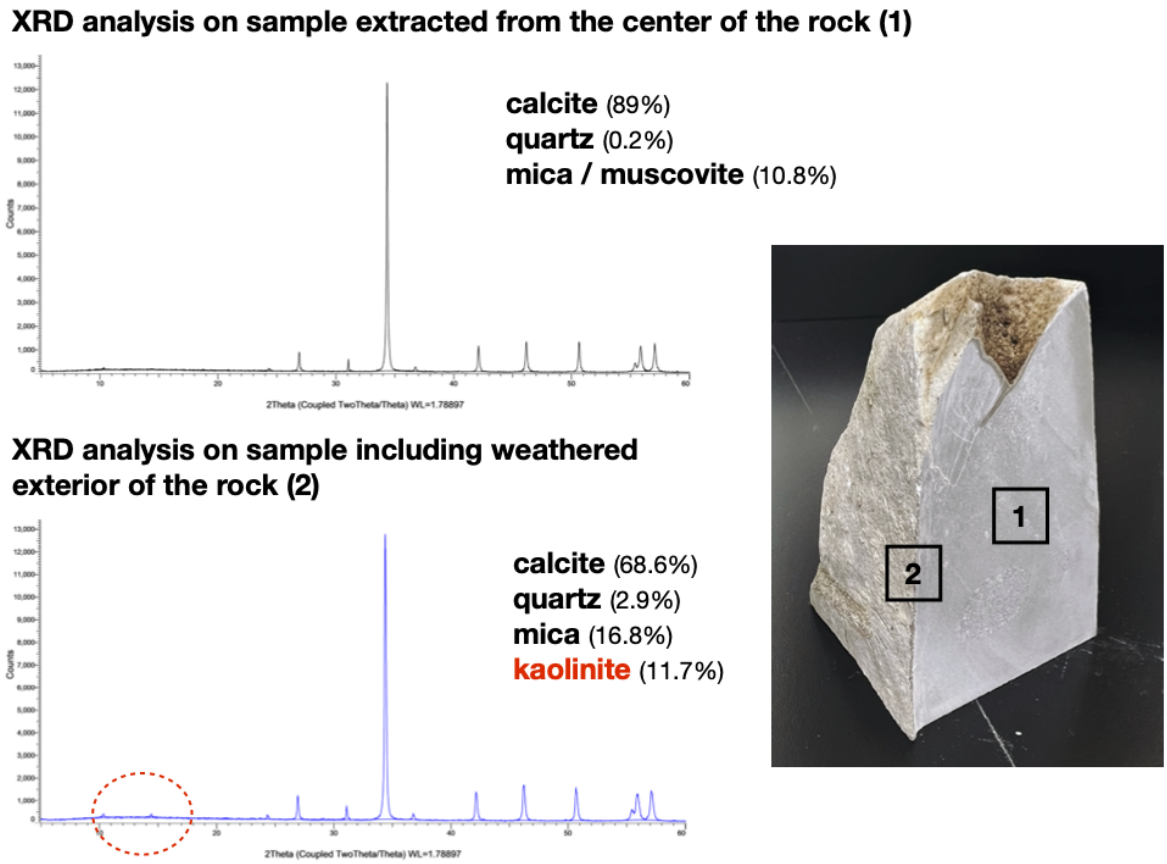

Figure 4.5: Mineral sampling locations and XRD peaks for rock matrix (1) and weathered surface (2) (Source: C Garing, UGA Geology Department).

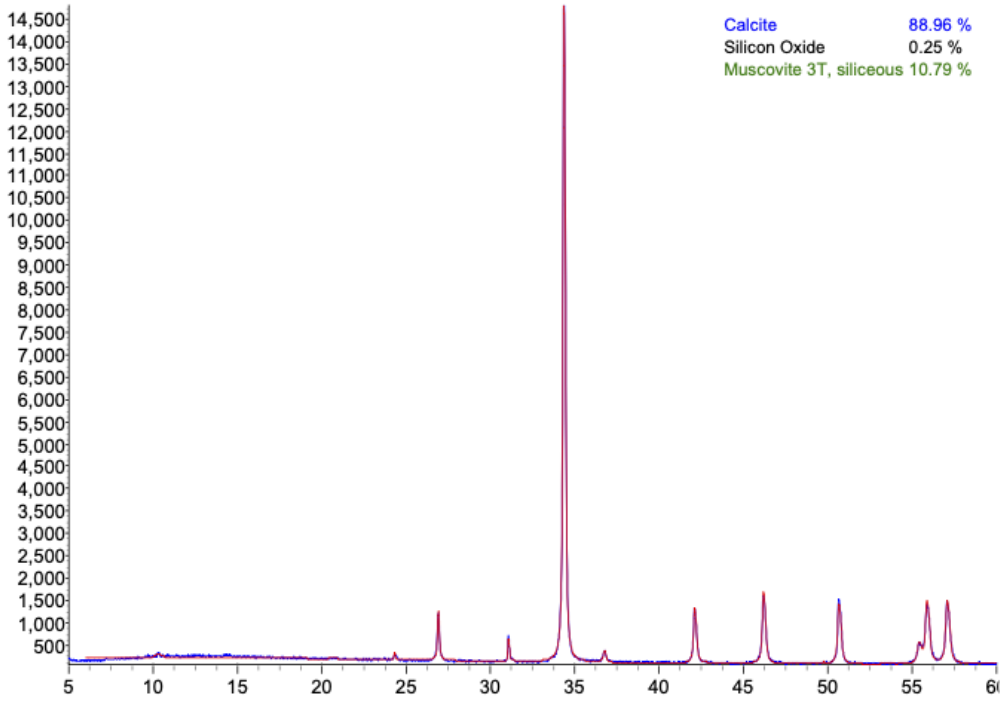

Figure 4.6: XRD spectrum of analyzed sample - rock matrix.

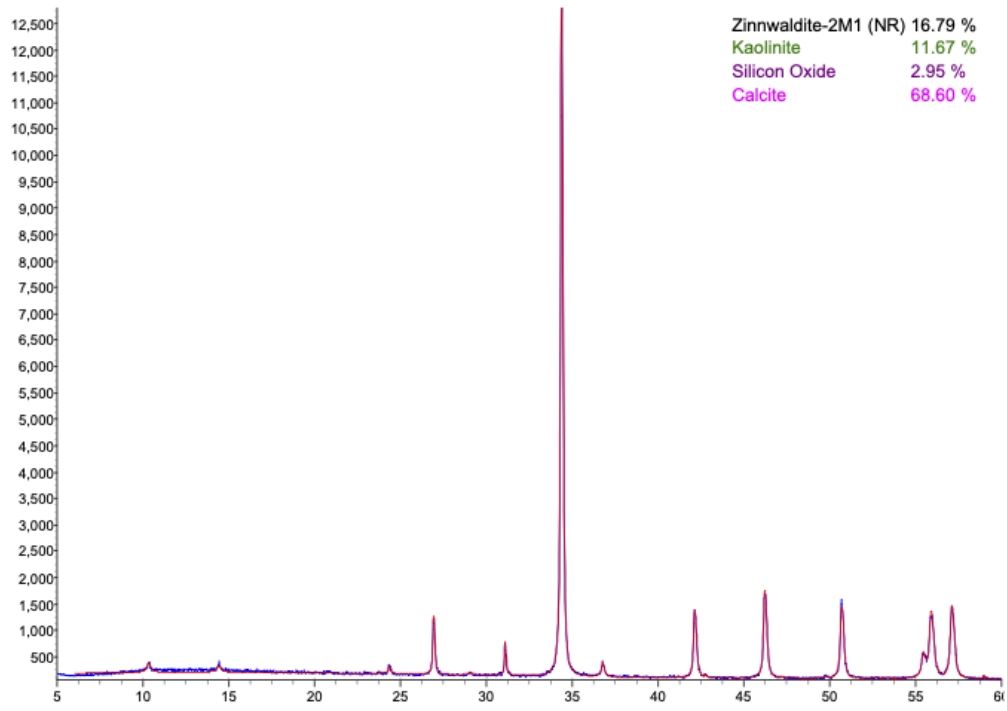

Figure 4.7: XRD spectrum of analyzed sample - weathered surface.

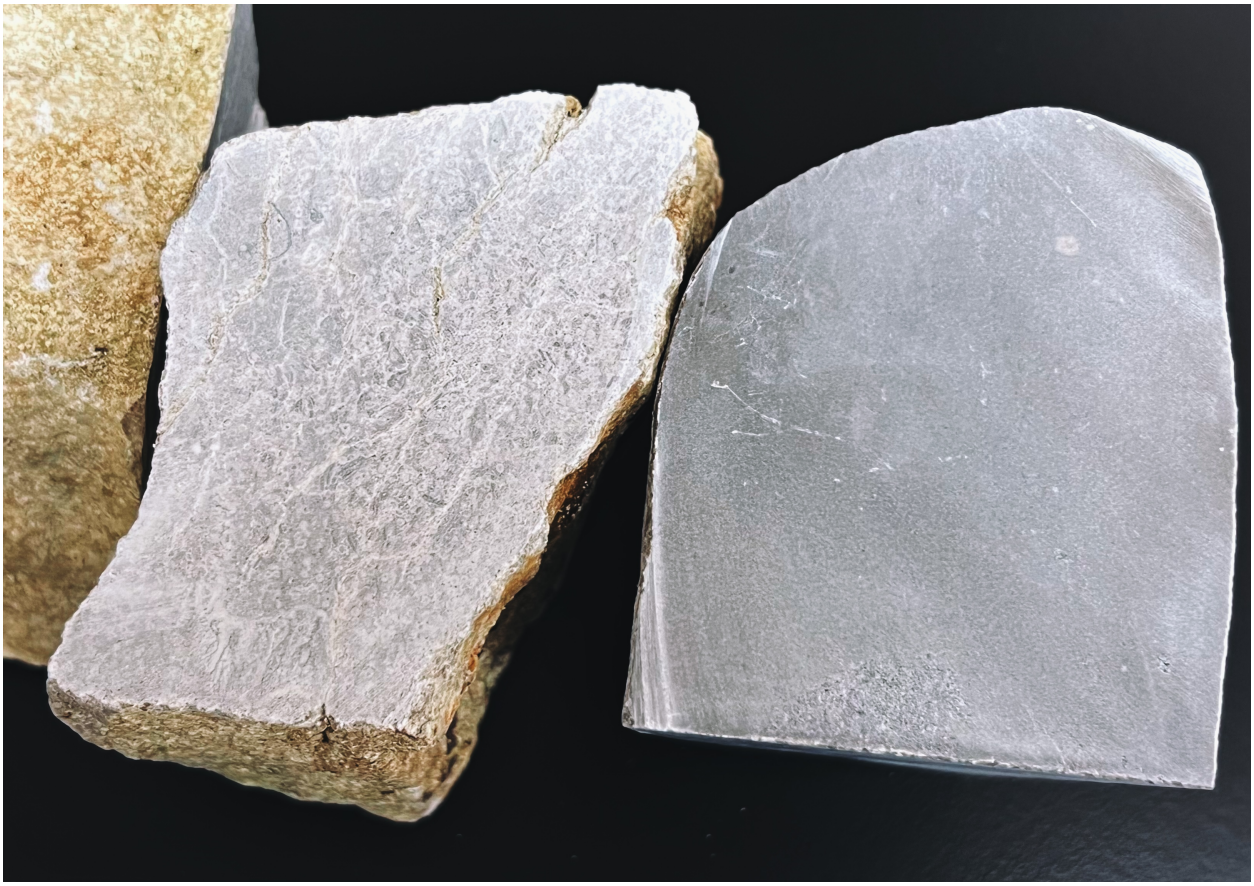

Figure 4.8: Tumbling Rock Cave outcrop, high calcite rock (left) and low porosity Monteagle Limestone (right). (Source: C Garing, UGA Geology Department)

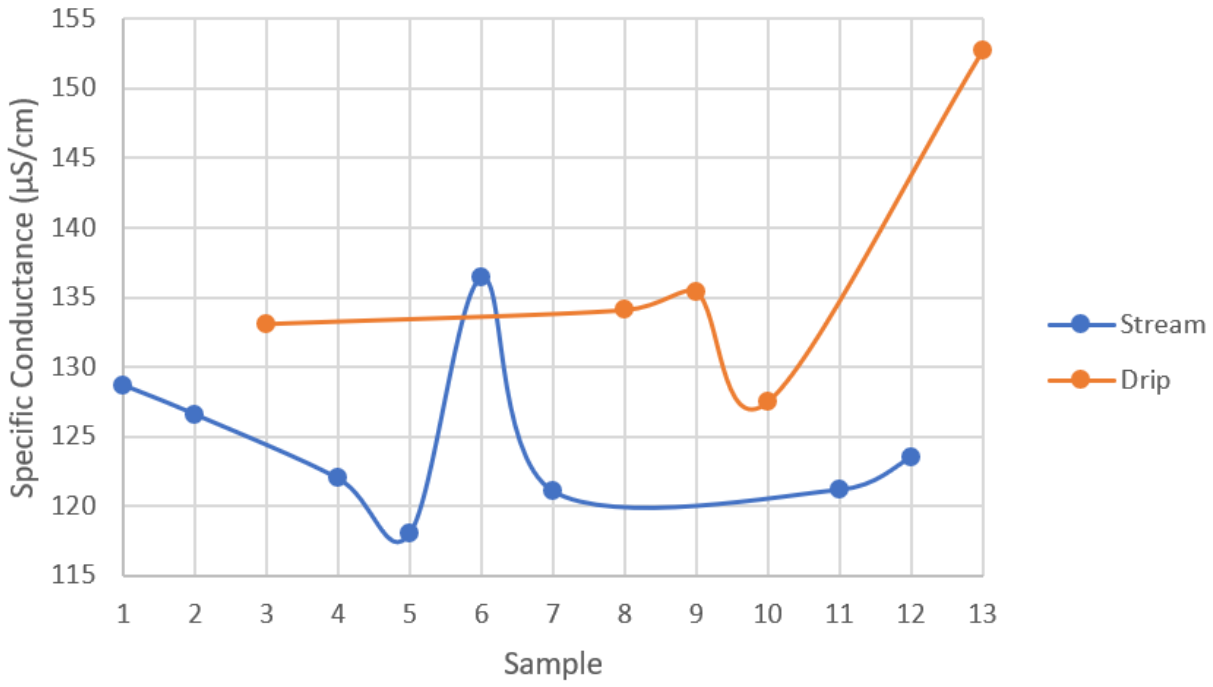

Figure 4.9: Specific conductance (μS/cm) for drips and streams within Tumbling Rock Cave - February 2023.

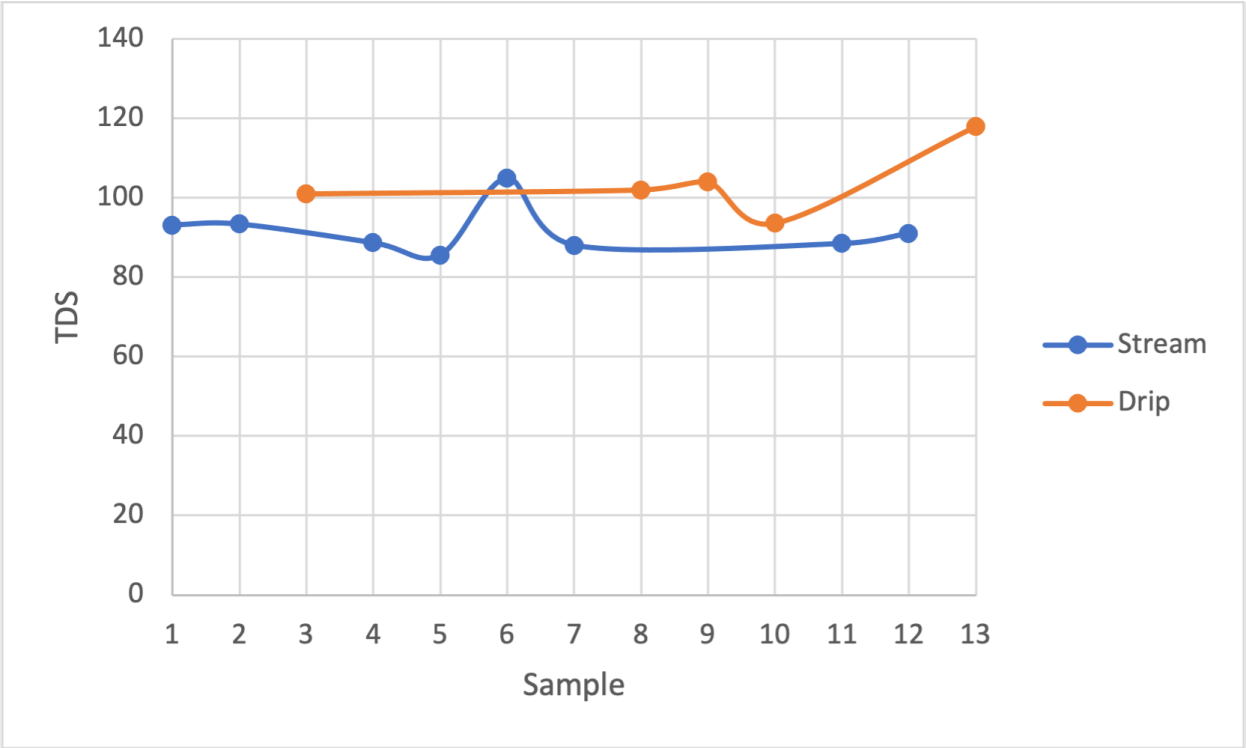

Figure 4.10: Total dissolved solids (mg/L) for drips and streams within Tumbling Rock Cave - February 2023.

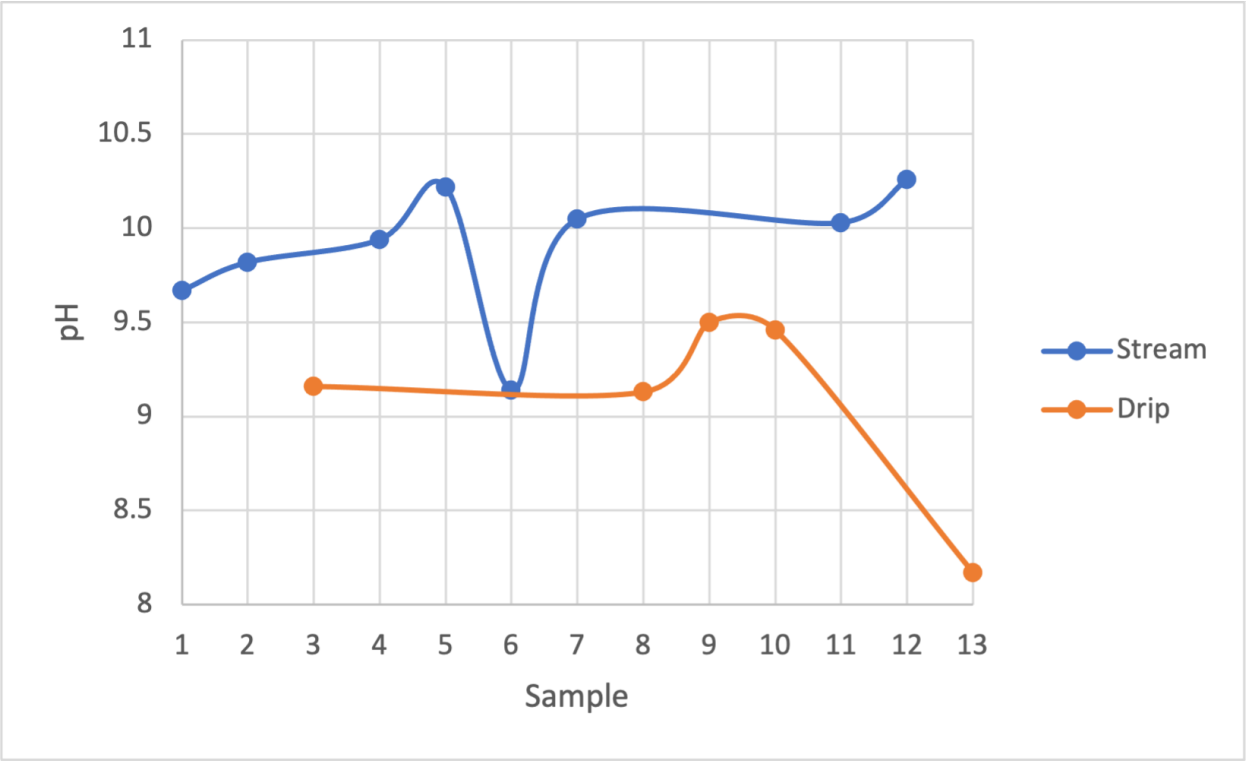

Figure 4.11: pH for drips and streams within Tumbling Rock Cave - February 2023.

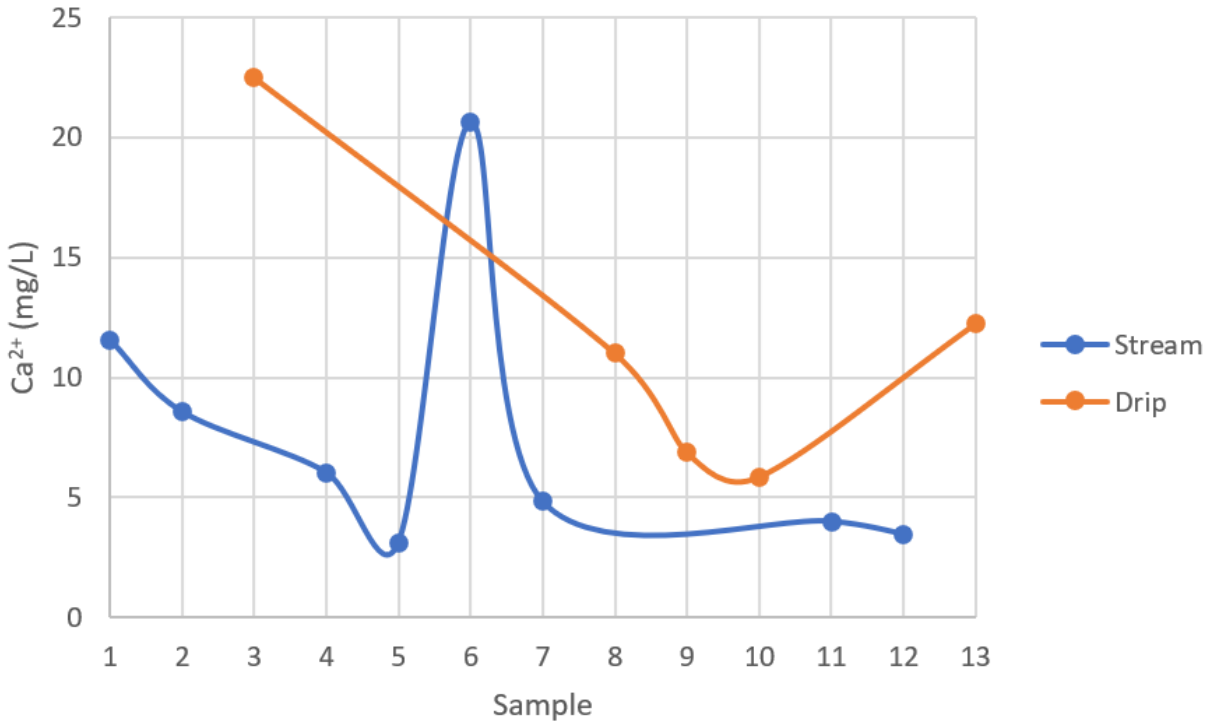

Figure 4.12: Calcium concentrations (mg/L) for drips and streams within Tumbling Rock Cave - February 2023.

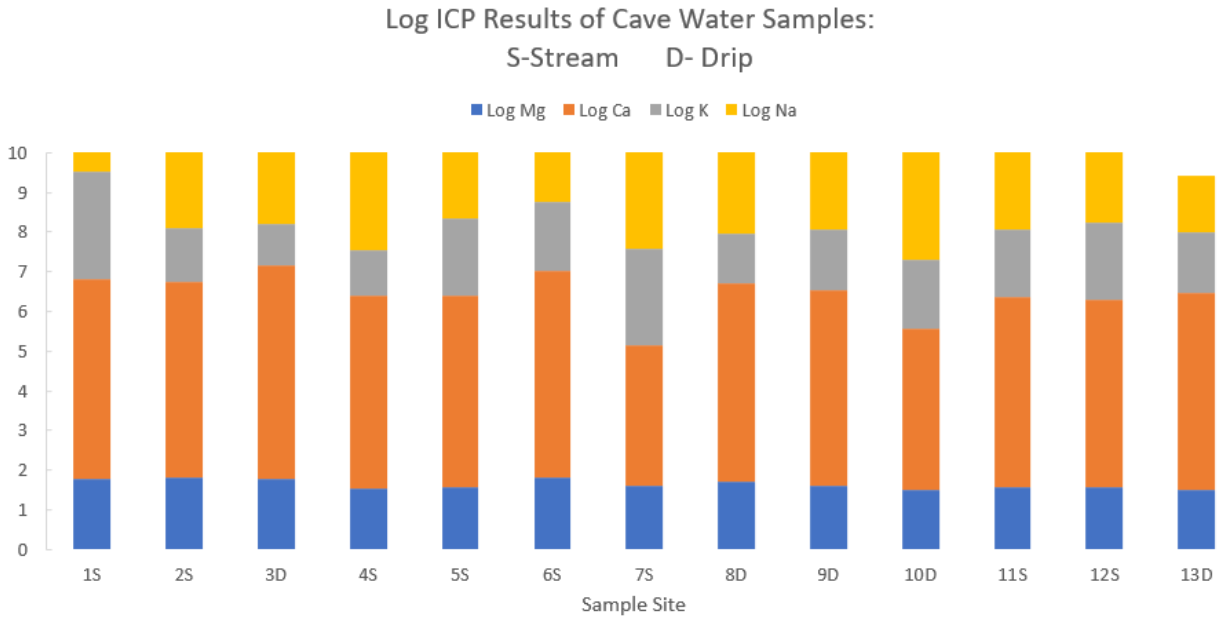

Figure 4.13: Log ICP results for major cations Identified from 13 water samples (drip and stream) - February 2023.

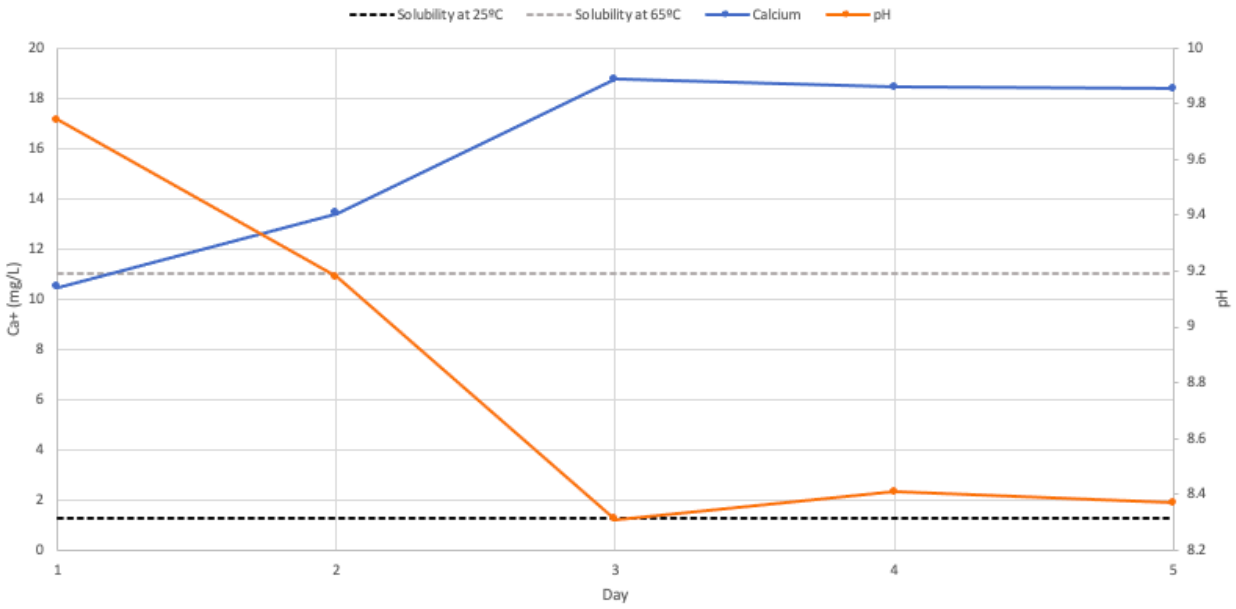

Figure 4.14: Relationship between calcium concentration (mg/L) and pH during a five-day leaching study - February 2023.

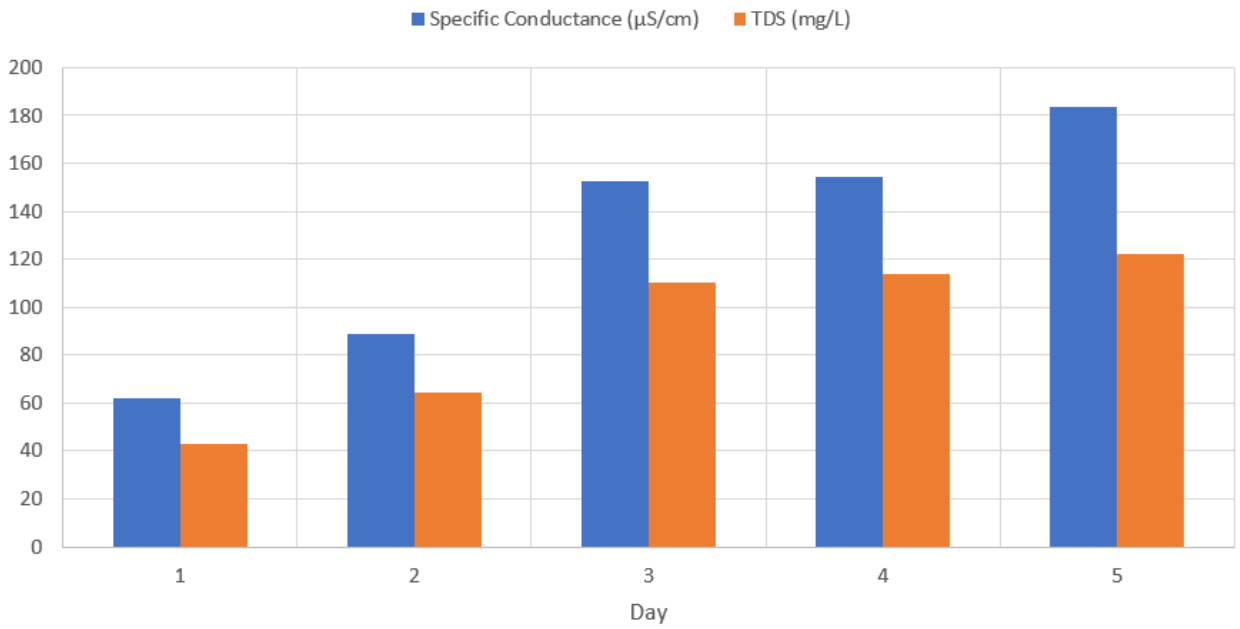

Figure 4.15: Relationship between specific conductance (μS/cm) and total dissolved solids (mg/L) during a five-day leaching study - February 2023.

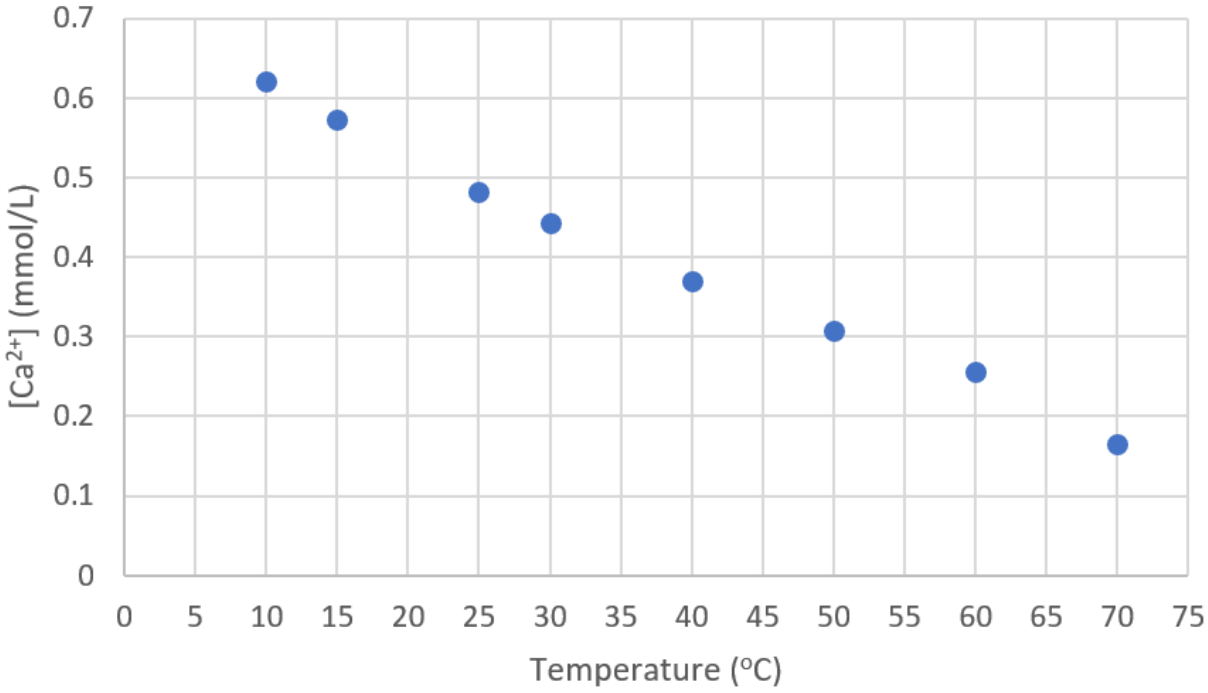

Figure 4.16: Theoretical calcium equilibrium kinetics vs temperature.

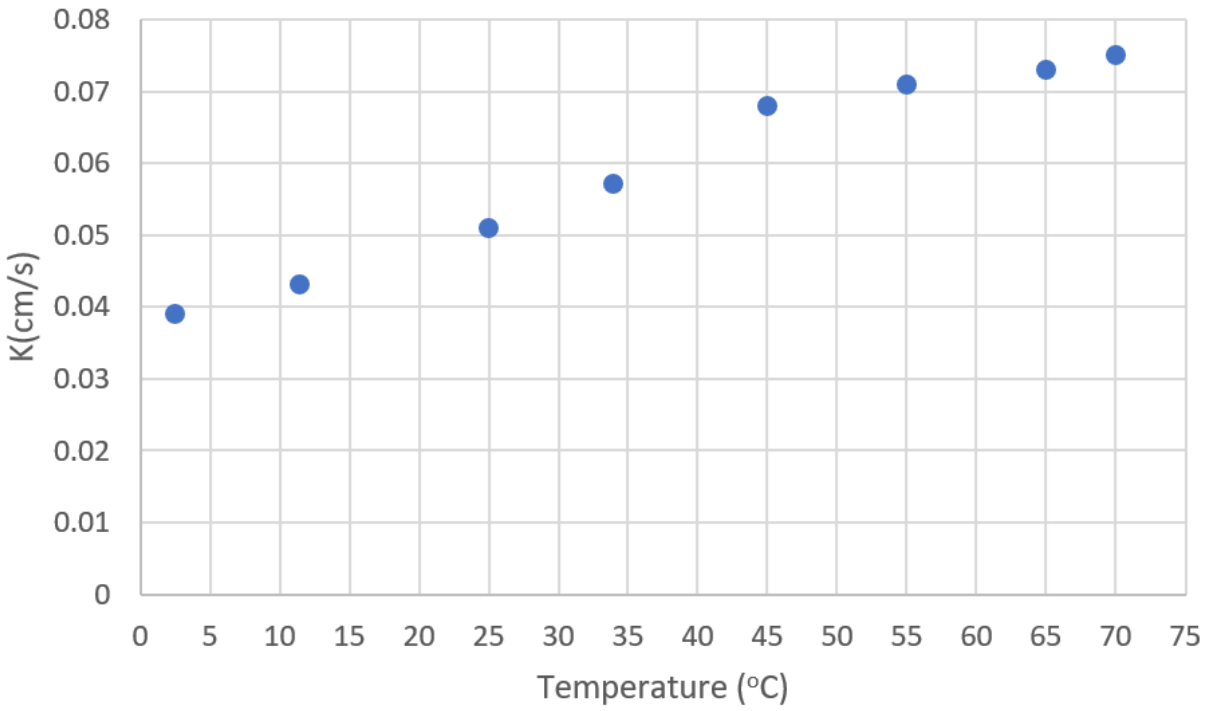

Figure 4.17: Theoretical dissolution kinetics vs temperature.

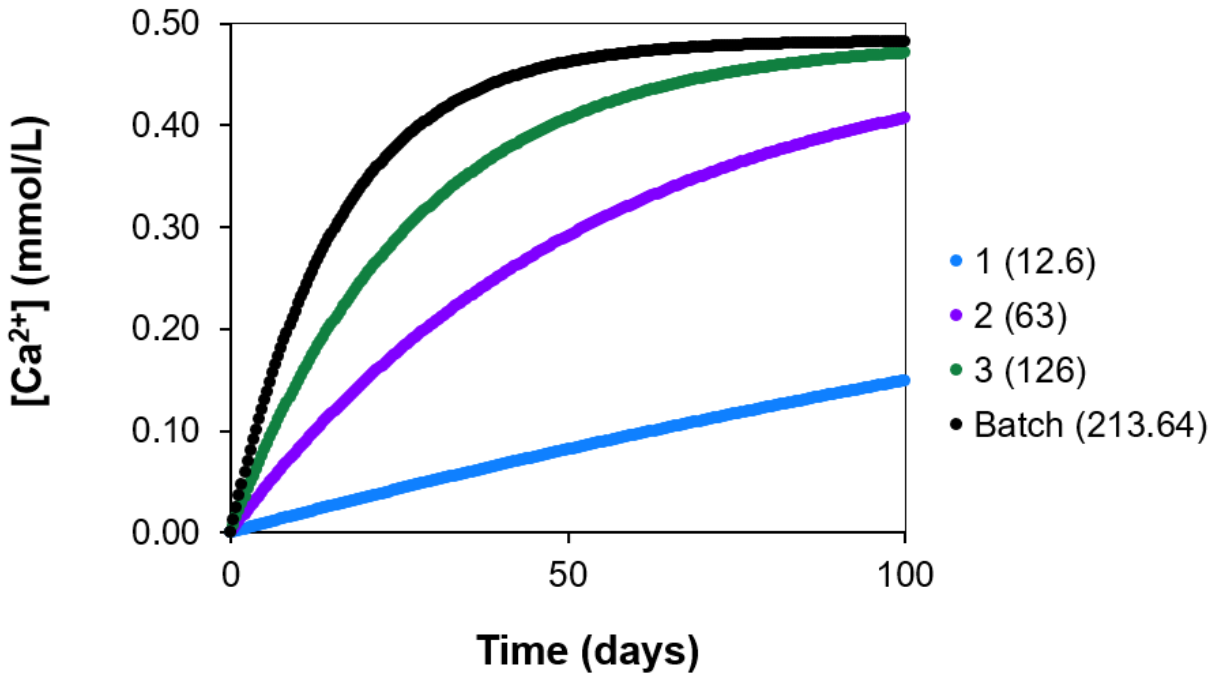

Figure 4.18: Calcium dissolution (mmol/L) at 25°C for four area/volume ratios. (Source: C Garing, UGA Geology Department)

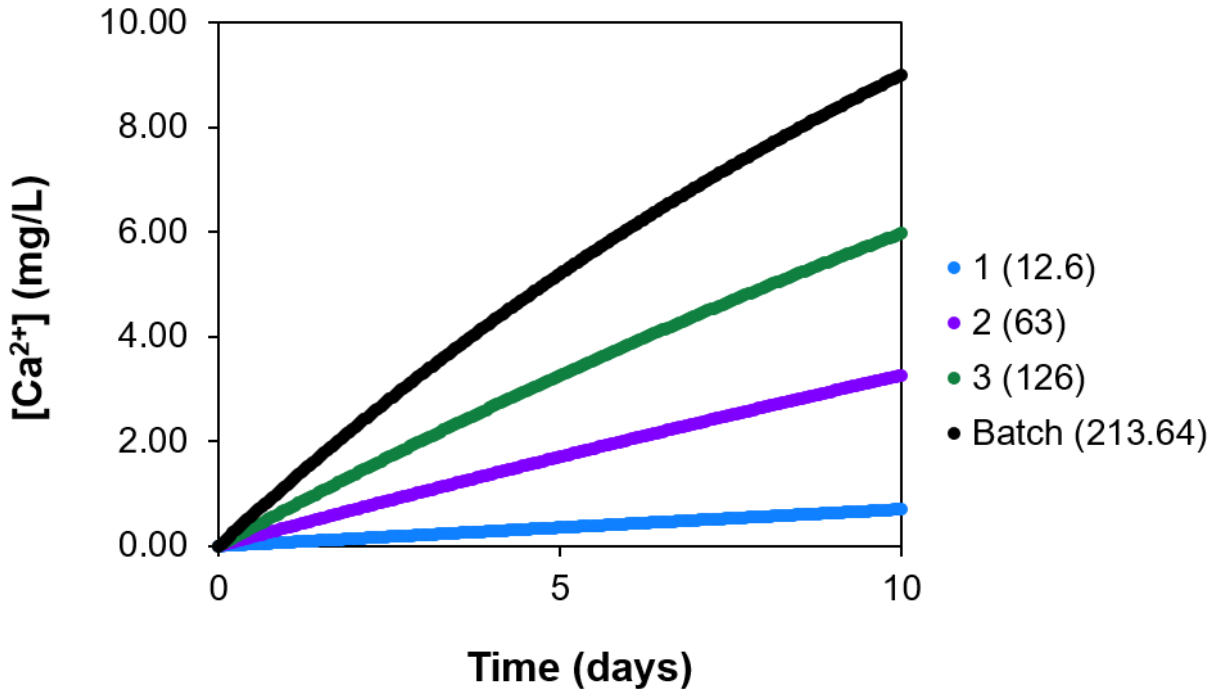

Figure 4.19: Calcium dissolution (mg/L) at 25°C for four area/volume ratios. (Source: C Garing, UGA Geology Department)

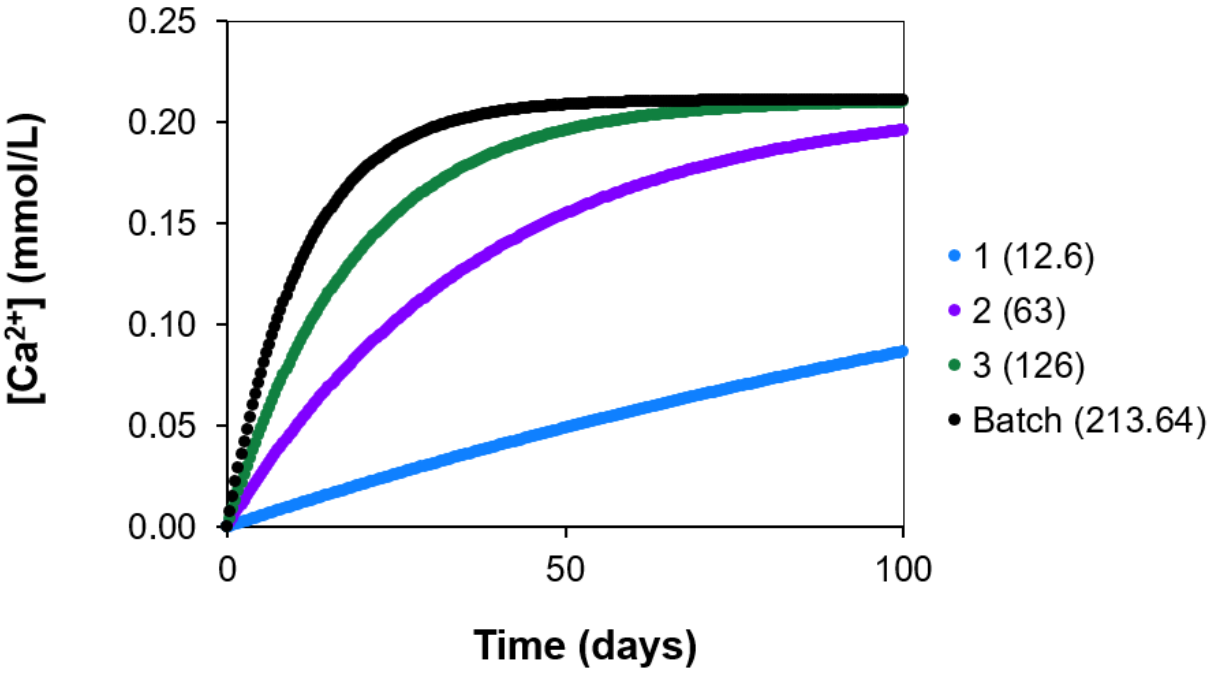

Figure 4.20: Calcium dissolution (mmol/L) at 65°C for four area/volume ratios. (Source: C Garing, UGA Geology Department)

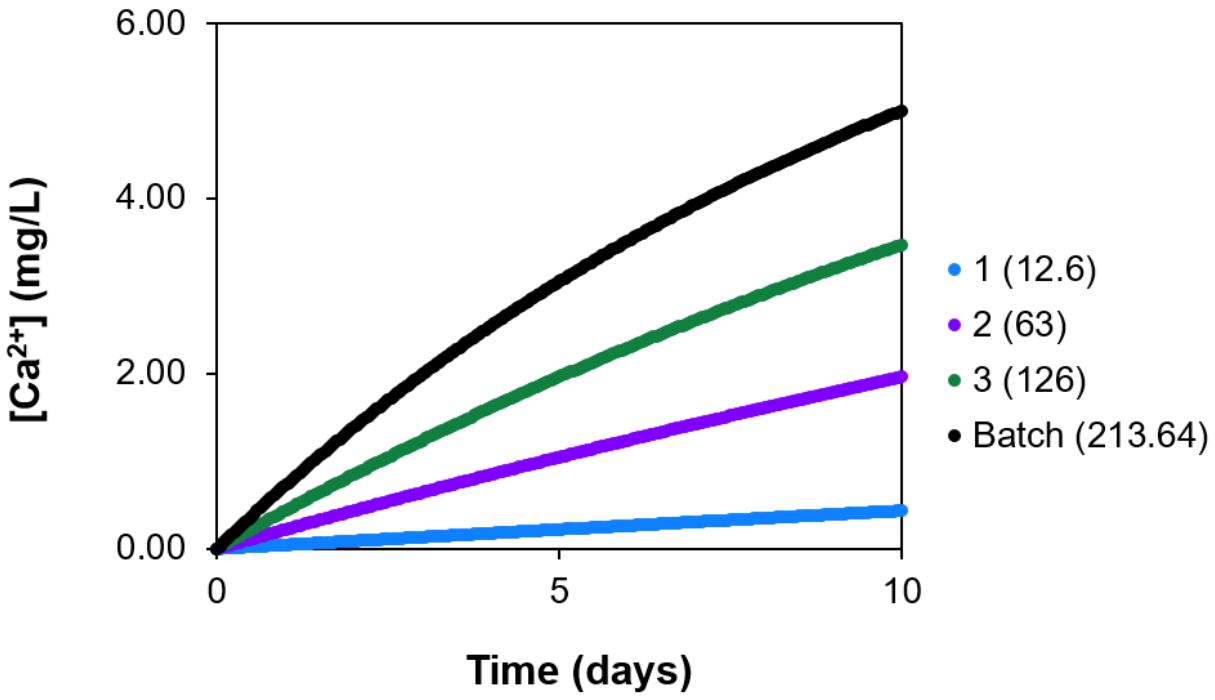

Figure 4.21: Calcium dissolution (mg/L) at 65°C for four area/volume ratios. (Source: C Garing, UGA Geology Department)

Chapter 5

Conclusion

This research focuses on developing and evaluating procedures for karst groundwater characterization by examining rock-water interactions. We hypothesize that:

1. The vulnerability to contamination in karst landscapes is a function of travel (or residence) times in the subsurface, with shorter residence times being more susceptible to contamination than longer pathways with greater residence times.

2. Rock elemental composition affects weathering rates through calcium dissolution so that water with longer subsurface travel times have greater calcium content than faster pathways.

3. Other water quality parameters (e.g., pathogens) are also affected by travel times, so that measuring carbonate concentrations provides information about the vulnerability to groundwater contamination.

4. Types of subsurface flows (rapid flow through streams in conduits, fracture, and drip flow) are related to travel times, so that knowledge of calcium concentrations from each provides information on their respective travel times.

Specific research objectives include:

1. Characterize parent rock material using X-ray diffraction (XRD), acid digestion, and laboratory mineral weathering procedures.

2. Characterize groundwater quality from precipitation, drips, subsurface streams, and spring discharge using Atomic Absorption Spectroscopy (AAS), Inductively Coupled

Plasma - Mass Spectrometry (ICP-MS) (i.e., Al, Ca, Fe, K, Mg, S), and chemical water quality parameters.

3. Use dissolved calcium concentrations to indicate calcite dissolution.
4. Estimate how temperature affects calcite dissolution rates from limestone samples using laboratory mineral weathering procedures and geochemical modeling.

Rock-water interactions were compared between conduits (rapid flow) and drips (slow flow) throughout the cave. We found a greater vulnerability to contamination in the conduits by lower concentrations of Ca^{2+}, SpC, and TDS. This leads us to believe conduits have shorter residence times and overall greater mixing. The drip samples presented greater concentrations of Ca^{2+}, SpC, and TDS, indicating longer residence times and greater water-rock interactions. This is consistent with previous studies shown by Normile 2022. In conclusion, travel times between conduits and drips indicate a greater susceptibility to contamination and pollution in the conduits.

The first objective of this study was to characterize the rock within Tumbling Rock Cave. Acid digestion revealed several elements critical to the dissolution of carbonate minerals. As expected, nearly all of the rock was identified as calcium, but other elements such as Aluminum, Iron, Potassium, Magnesium, and Sulfur presented insight into dissolution factors and the presence of secondary minerals. Iron and sulfur present in the water can lead to acidic conditions, increasing the dissolution rates. Aluminum, Potassium, and Magnesium lead us to believe weathering of the calcite is leading to the formation of secondary minerals. XRD results allowed for interpretations of both the parent material and weathered rock. These results confirmed chemical weathering of limestone was present.

The second objective was to characterize the groundwater quality of the cave. The meteorology in the region leads us to believe the cave sees similar responses in flow to the local precipitation. Using analytical methods, AA and ICP, water quality results on elemental and ionic concentrations supported water-rock interactions by the presence of dissolved calcium.

The final objective was to understand calcite dissolution in a laboratory setting and through theoretical computation. The leaching experiment showed similar responses to the theoretical calculations and portrayed dissolution. Geochemistry helped identify theoretical rates of dissolution and give insight into reactions occurring within the cave.

5.1 Limitations

Several limitations impacted this research in both time and space. The biggest limitation to this study was the location of the field site. Routine sampling was difficult because the location of the field site was over 320 km (200 mi) from UGA and the laboratory. This research was also limited by the frequency sampling in both rock and water samples. Ideally, sampling across multiple lithologies and throughout the Monteagle limestone would allow for better characterization of the mineralogy. The leaching study was limited by the instruments available. Ideally, a leaching study would be performed in a more controlled environment to maintain temperature, and humidity, and minimize evaporation. Lastly, the geochemical modeling was limited by the available resources and training for students at UGA.

5.2 Future Research

This research can be employed in future studies on Tumbling Rock Cave and other caves in order to characterize geologic formations and water quality within a cave system.

Rock and mineral characterization could be performed on a broader range of rock samples from various locations within the cave. This could provide further insight into the formation of secondary minerals and the dissolution processes within the cave. Sampling across varying lithologies could validate thicknesses and expand on the geologic history. Additionally, characterizing the rock and soil above the cave could give a broader insight into the landscape and formation of the cave.

In future studies, increasing the frequency of water sampling and locations throughout the cave could be substantial in understanding the water-rock interactions. We can better validate trends between drips and streams, with increased sampling. This can also help to characterize seasonal variability in water quality and flow. In situ water quality measurements would be ideal to avoid contamination or disturbance during capture, storage, and laboratory analysis. Continuous stage and flow measurements in drips and streams should be employed within the cave, to better understand the flow dynamics and their response to precipitation events.

Leaching experiments could be improved in a number of ways. Leaching at a constant temperature throughout the five-day period would allow for experimental dissolution rates to be determined. Experiments using different pressures to show how dissolution changes. Experiments at different particle sizes to show how surface area affects water-rock interactions. Other parameters to consider could involve wet/dry cycles, humidity, stirring, sealed, etc...

In conclusion, addressing these limitations and incorporating additional sampling, analytical techniques, and experiments would lead to a more comprehensive characterization of Tumbling Rock Cave.

Chapter 6

References

Adams, G. I., Butts, C., Stephenson, L. W., Cooke, W. (1926). Geology of Alabama. United States. Special Report Number 14. Geological Survey of Alabama, University of Alabama. Birmingham Printing Company, Publishers, 312 pp. https://books.google.com

Appelo, C. A. J., and Postma, D. (2004). Geochemistry, Groundwater and pollution. CRC press. ISBN: 978-0415364287

Arbel, Y., Greenbaum, N., Lange, J., and Inbar, M. (2010). Infiltration processes and flow rates in developed karst vadose zone using tracers in cave drips. Earth Surface Processes and Landforms, 35(14), 1682-1693. https://doi.org/10.1002/esp.2010

Baker, A., Barnes, W. L., Smart, P. L. (1997). Variations in the discharge and organic matter content of stalagmite drip waters in Lower Cave, Bristol. Hydrological Processes, 11(11), 1541-1555. https://doi.org/10.1002/(SICI)1099-1085(199709)11:11<1541::AID-HYP484>3.0.CO;2-Z

Chou, L. E. I., Garrels, R. M., Wollast, R. (1989). Comparative study of the kinetics and mechanisms of dissolution of carbonate minerals. Chemical geology, 78(3-4), 269-282. https://doi.org/10.1016/0009-2541(89)90063-6

Chu, H., Wei, J., Wang, R., Xin, B. (2017). Characterizing the interaction of groundwater and surface water in the karst aquifer of Fangshan, Beijing (China). Hydrogeology Journal, 25(2), 575. https://doi.org/10.1007/s10040-016-1507-7

Creed, J. T., Brockhoff, C. A., Martin, T. D. (1994) US-EPA Method 200.8: determination of trace elements in waters and wastes by inductively coupled plasma-mass spectrometry, in Environmental Monitoring Systems Laboratory Office of Research and Development, Revision 5.4 EMMC Version, U.S. Environmental Protection Agency, Cincinnati, Ohio, USA. https://www.epa.gov/sites/default/files/2015-08/documents/method_200-8_rev_5-4_1994.pdf

Currens, J. C. (1999). Mass flux of agricultural nonpoint-source pollutants in a conduit-flow-dominated karst aquifer, Logan County, Kentucky. Kentucky Geological Survey Report of Investigations. 3. https://uknowledge.uky.edu/kgs_ri/3

Geological Survey of Alabama (2013). Geologic Map of the Scottsboro 7.5-minute Quadrangle, Jackson County Alabama. https:www.gsa.state.al.us/gsa/geologic/mapping

Groves, C., Meiman, J. (2005). Weathering, geomorphic work, and karst landscape evolution in the Cave City groundwater basin, Mammoth Cave, Kentucky. Geomorphology, 67(1-2), 115-126. https://doi.org/10.1016/j.geomorph.2004.07.008

Handford, C. R. (1978). Monteagle Limestone (Upper Mississippian)—oolitic tidal-bar sedimentation in southern Cumberland Plateau. AAPG Bulletin, 62(4), 644-656. https://doi.org/10.1306/C1EA4E1E-16C9-11D7-8645000102C1865D

Islam, Jahangir, and Naresh Singha (2004)l. "A laboratory study of landfill-leachate transport in soils." Water research 38.8 (2004): 2035-2042. https://doi.org/10.1016/j.watres.2004.01.024

Johnson, J.(2004). Understanding changing carbonate chemistry of the ocean requires an understanding of the behavior of CO2 and how it affects carbonate equilibrium. Among other processes, dissolution of atmospheric CO2 affects carbonate mineral precipitation and oceanic life. Thus, it is important to consider how CO2 input changes the oceans' chemistry and how continued input.

Li, L., Steefel, C. I., Yang, L. (2007). Mineral dissolution kinetics at the pore scale (No. LBNL-63303). Lawrence Berkeley National Lab (LBNL), Berkeley, CA (United States). https://escholarship.org/uc/item/9nq4x883

Lin, J., Liu, Y., Yang, Y., Hu, Z. (2016). Calibration and correction of LA-ICP-MS and LA-MC-ICP-MS analyses for element contents and isotopic ratios. Solid Earth Sciences, 1(1), 5-27. https://doi.org/10.1016/j.sesci.2016.04.002

Morse, J. W., and Arvidson, R. S. (2002). The dissolution kinetics of major sedimentary carbonate minerals. Earth-Science Reviews, 58(1-2), 51-84. https://doi.org/10.1016/S0012-8252(01)00083-6

Neven, K., Sorab, P. (2021). Modeling of groundwater flow and transport in coastal karst aquifers. Hydrogeology Journal, 29(1), 249-258. https://doi.org/10.1007/s10040-020-02262-3

Normile, Z. (2022) Evaluating Risk Pathways for Groundwater Contaminants on a Karstic Landscape

Olesik, J. W. (1991). Elemental analysis using icp-oes and icp/ms. Analytical Chemistry, 63(1), 12A-21A. https://pubs.acs.org/doi/pdf/10.1021/ac00001a001

Panagopoulos, G., Lambrakis, N. (2006). The contribution of time series analysis to the study of the hydrodynamic characteristics of the karst systems: Application on two typical karst aquifers of Greece (Trifilia, Almyros Crete). Journal of hydrology, 329(3-4), 368-376. https://doi.org/10.1016/j.jhydrol.2006.02.023

Plummer, L. N., Wigley, T. M. L., Parkhurst, D. L. (1978). The kinetics of calcite dissolution in CO_2-water systems at 5 degrees to 60 degrees C and 0.0 to 1.0 atm CO_2. American journal of science, 278(2), 179-216. https://doi.org/10.2475/ajs.278.2.179

Pokrovsky, O. S., Golubev, S. V., Schott, J., Castillo, A. (2009). Calcite, dolomite and magnesite dissolution kinetics in aqueous solutions at acid to circumneutral pH, 25 to 150 C and 1 to 55 atm pCO2: New constraints on CO2 sequestration in sedimentary basins. Chemical geology, 265(1-2), 20-32. https://doi.org/10.1016/j.chemgeo.2009.01.013

Schweitzer, C. J., Dey, D. C. (2013). Logging intensity impact on small oak seedling survival and growth on the Cumberland Plateau in Northeastern Alabama. Southern Journal of Applied Forestry, 37(2), 113-121. https://doi.org/10.5849/sjaf.11-003

(SCCi), Southeastern Cave Conservancy, Incorporated (2023). Schematic of karst systems in the Cumberland escarpment

Sutherland, C. (2021). Caves of KTAG. https://www.flickr.com/photos/chucksutherland/50875573288

Swingle, G. D. (1965). An introduction to the geology of the southern Appalachians. 1965 ACA-MSA Fieldtrip Guidebook. http://www.minsocam.org/msa/OpenAccess_publications/MSA_ACA_fieldtrip/MSA_ACAfieldtrip_Intro.pdf

Taylor, B. E., Wheeler, M. C., and Nordstrom, D. K. (1984). Stable isotope geochemistry of acid mine drainage: Experimental oxidation of pyrite. Geochimica et Cosmochimica Acta, 48(12), 2669-2678. https://doi.org/10.1016/0016-7037(84)90315-6

Thomas, W. A. (1972). Mississippian Stratigraphy of Alabama. Monograph 12, Division of Paleontology and Stratigraphy, Geological Survey of Alabama, 132 pp. https://www.gsa.state.al.us/Home/DownloadPubDocument/?path=Monographs&fileName=M012.pdf

Thomas, W. A., Mack, G. H. (1982). Paleogeographic relationship of a Mississippian barrier-island and shelf-bar system (Hartselle Sandstone) in Alabama to the Appalachian-Ouachita erogenic belt. Geological Society of America Bulletin, 93(1), 6-19. https://doi.org/10.1130/0016-7606(1982)93%3C6:PROAMB%3E2.0.CO;2

Tooth, Anna F., and Ian J. Fairchild. "Soil and karst aquifer hydrological controls on the geochemical evolution of speleothem-forming drip waters, Crag Cave, southwest Ireland." Journal of Hydrology 273.1-4 (2003): 51-68. https://doi.org/10.1016/S0022-1694(02)00349-9

USDA-NRCS (2019). Web Soil Survey https://websoilsurvey.nrcs.usda.gov/app/

USEPA Method 3052 (1995) "Microwave assisted acid digestion of siliceous and organically based matrices," in Test Methods For Evaluating Solid Waste, US Environmental Pro-

tection Agency, Washington, DC, USA, 3rd edition. https://www.epa.gov/sites/default/files/2015-12/documents/3052.pdf

USGS (1948). 7.5-minute Quadrangle, Mud Creek, Alabama. https://prd-tnm.s3.amazonaws.com/StagedProducts/Maps/HistoricalTopo/PDF/AL/24000/AL_Mud%20Creek_304633_1948_24000_geo.pdf

USGS (2021). PHREEQC Version 3 https://www.usgs.gov/software/phreeqc-version-3

USGS (2023). Stream Stats Application https://www.usgs.gov/streamstats

White, W. B. (1988). Geomorphology and hydrology of karst terrains. United Kingdom: Oxford University Press. https://digitalcommons.usf.edu/kip_articles/2160

White, W. B. (2002). Karst hydrology: Recent developments and open questions. Engineering geology, 65(2-3), 85-105. https://doi.org/10.1016/S0013-7952(01)00116-8

Wu, P., Tang, C., Zhu, L., Liu, C., Cha, X., Tao, X. (2009). Hydrogeochemical characteristics of surface water and groundwater in the karst basin, southwest China. Hydrological Processes: An International Journal, 23(14), 2012-2022. https://doi.org/10.1002/hyp.7332

Appendix A

Sample Preparation

Limestone samples are first washed with a coarse bristle sponge to remove any scum or debris on the surface. The Limestone samples are then cut into small fractions using a diamond tipped rotary saw shown in Figure A.1. The small fractions of rock (Figure A.2) are then crushed using a mortar and pestle shown in Figure A.3. Samples were crushed until they pass through a 0.6096-cm sieve shown Figure A.4 in order to increase the surface area. The crushed and sieved material is then put in the oven at 230°C for four hours in order to sterilize and remove all moisture. Figure A.5 shows an exposed fracture along a preferential flow path where dissolution is likely occurring.

Figure A.1: Cutting rock samples using diamond saw blade.

Figure A.2: Cut rock samples.

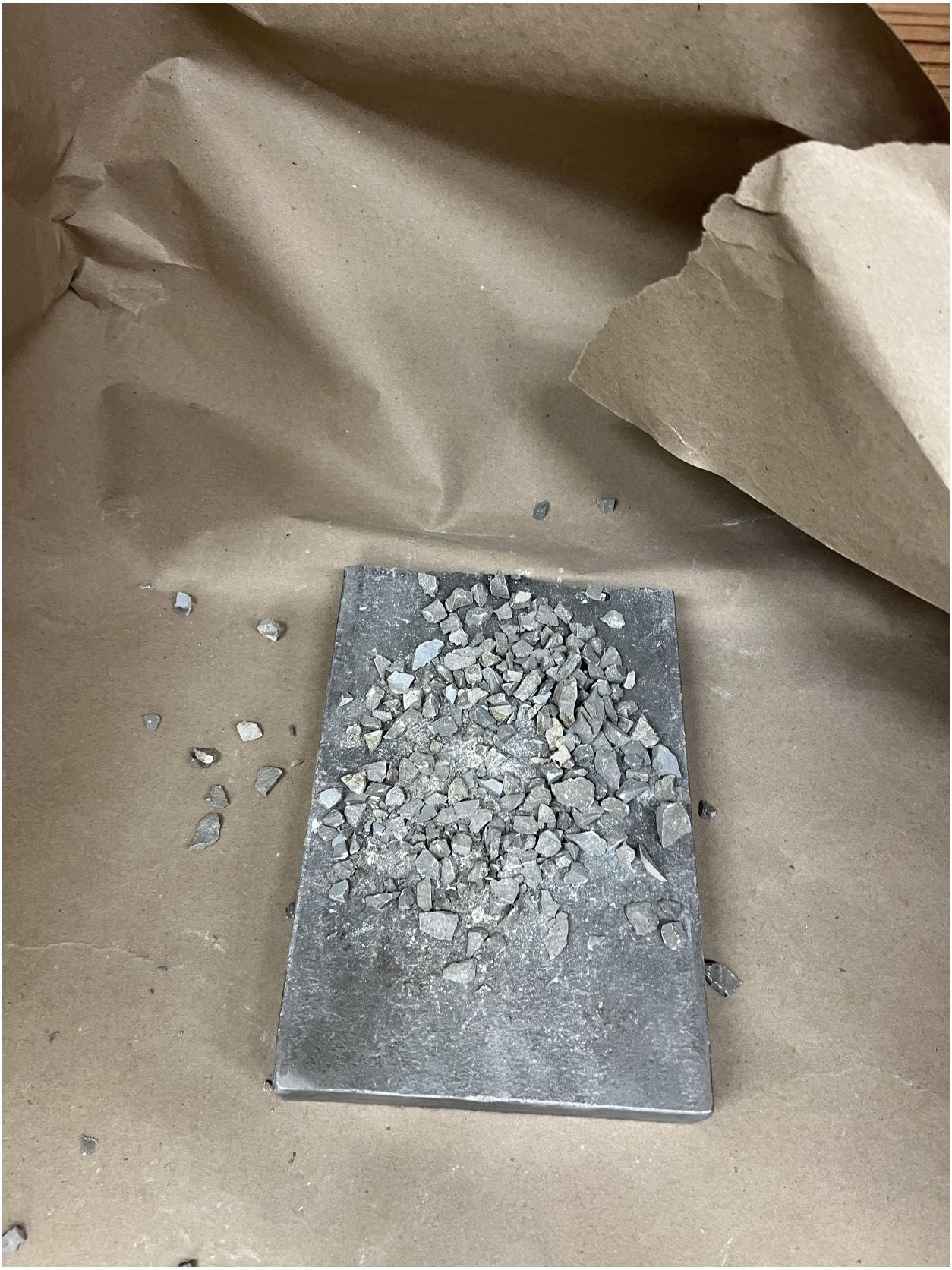

Figure A.3: Crushing rock samples with a mortar and pestle.

Figure A.4: Crushed rock samples passing through 0.67-cm sieve.

Figure A.5: Fracture exposed from cutting rock.